Geomorphology 498 (2026) 110172

Contents lists available at ScienceDirect

Geomorphology

journal homepage: www.journals.elsevier.com/geomorphology

# An extended kinematic inventory, magnitude-frequency curves, and damage assessment of rock slope failures in the central Spanish Pyrenees

J. Guerrero [a,*], M. Guerra [a], G. Desir [a], A. Serreta [b], Y. Thiery [c], P. Lucha [d]

[a] Earth Science Department, Universidad de Zaragoza, Spain
[b] Escuela Politécnica Superior de Huesca, Universidad de Zaragoza, Spain
[c] Bureau de Recherche Géologique et Minières, DRP, R3C, Europarc, France
[d] Science Teaching Department, Universidad de Zaragoza, Spain

ARTICLE INFO

*Keywords:*
Landslide inventory
Conditioning factors
Large landslide
Landslide damage
Weathering
Rock slope failure
SPIRAL

ABSTRACT

A new inventory of rock slope failures (RSFs) compiled in the central Spanish Pyrenees within the framework of the SPIRAL Project has identified 1232 RSFs, yielding a relatively low spatial density of 0.11 events per km$^2$. These RSFs exhibit very slow to extremely slow average displacement rates, ranging from 5 mm to 75 mm per year. Rock slides and earthflows are the most prevalent failure types, accounting for over 93% of the total, whereas rock slope deformations (RSDs), composite failures, and rock avalanches are comparatively rare. This predominance of rock slides and earthflows results in a shallower magnitude–frequency distribution relative to other mountainous regions. Lithology, glacial debuttressing, and slope angle are identified as the most influential conditioning factors. Most RSFs occur on slopes between 20° and 30°, especially in deglaciated settings and in bedrock composed of fine-grained, low-strength lithologies, such as turbidites, slates, marls, and evaporitic sequences, where weathering plays a critical role in promoting slope instability. Unfortunately, these relatively moderate slopes, which often correspond to relict landslide deposits, provided favourable conditions for the establishment of at least 25 human settlements in the past. These communities are now under threat and will require multimillion-euro investments to stabilize active movements. Furthermore, 41 RSFs intersect communication and irrigation networks, 138 affect ski resort infrastructures, 94 compromise paved roads, and 29 pose risks to dam safety. The estimated direct costs associated with active RSFs already exceed €152 million, and additional substantial mitigation efforts are anticipated in the near future.

## 1. Introduction

Landslides are among the most frequent and globally widespread natural hazards, resulting in substantial human casualties and economic losses each year (Schuster and Highland, 2001). Recent studies suggest that their true impact remains significantly underestimated (Sim et al., 2022). According to current estimates, landslides are responsible for approximately 4000 fatalities annually and economic losses amounting to billions of dollars worldwide (Froude and Petley, 2018; Pollock and Wartman, 2020). In Europe alone, over a 20-year period, an average of 68 fatalities and €4.7 billion in annual damages were reported across 476 fatal landslide events (Haque et al., 2016). According to the same study, Spain ranks third among European countries in economic losses and fifth in fatalities due to landslides. In addition, the European landslide susceptibility map (Wilde et al., 2018) indicates that the Pyrenees is among the five main European landslide hotspots (Jaedicke et al., 2014).

In Spain, the BDMOVES inventory (Base de datos de Movimientos del Terreno), developed by the Geological Survey of Spain (IGME, 2025), currently represents the most comprehensive national landslide database. It includes 4386 documented slope instability events of all types, accounting for several hundred fatalities and million euros in historical economic losses (Corominas et al., 2025). However, in the Pyrenees, the number of inventoried landslides remains sparse (IGME, 2025), clearly underestimating their true impact in this mountainous region where landslides Notable historical landslide events in the Spanish Pyrenees include represent a major geomorphic process, frequently associated with significant economic damages, abandonment of settlements, and severe infrastructure disruption. Notable historical landslide events in the Spanish Pyrenees include the following: (1) the 1373 Monclús

* Corresponding author.
*E-mail address:* jgiturbe@unizar.es (J. Guerrero).

https://doi.org/10.1016/j.geomorph.2026.110172
Received 14 November 2025; Received in revised form 7 January 2026; Accepted 9 January 2026
Available online 13 January 2026

translational rockslide (~12 $hm^3$), triggered by an earthquake, which completely destroyed the village of Monclús (Zarroca et al., 2013); (2) the 1714 Inza earthflow, which advanced at an average rate of 20 m/day and obliterated the village of Inza (Aparicio Valls et al., 1987); (3) the 1940s Salinas de Jaca rockslide, which led to the abandonment of the town (Gutiérrez et al., 2014); (4) the 1881 Puigcercós rockslide (~5 × $10^6$ $m^3$), which destroyed several houses and prompted the abandonment of the village (Khazaradze et al., 2020); and (5) the 1982 reactivation of the Pont de Bar earthflow, triggered by intense rainfall, which destroyed a 300 m section of the national highway between Puigcerdà and La Seu d'Urgell, severely damaged the village of Pont de Bar, and ultimately led to its abandonment (Corominas, 2006).

Currently, the central sector of the Pyrenees, including the French-Spanish border, is affected by a large number of landslides. Among these, rock slope failures (RSFs) defined in the literature as an umbrella term for landslides involving bedrock (Jarman et al., 2014; Jarman and Harrison, 2019), represent the most frequently occurring type of mass movement. This region is characterized by a predominance of weak rocks ranging from the Paleozoic to the Neogene, which play a key role in slope instability and are the primary conditioning factor influencing the spatial distribution and typology of RSFs. Many of them are characterized by deep-seated shear surfaces and volumes exceeding several tens of $hm^3$. These phenomena directly impact critical cross-border infrastructures, settlements, reservoirs, and ski resorts, often implying costly engineering mitigation measures and posing a substantial threat to human lives.

The aim of this study is to present a new, high-resolution kinematic RSF inventory for the Aragón region (NW Spain) in the central Pyrenees, developed within the framework of the SPIRAL project (Interreg-POCTEFA program 2021–2027, EFA039/01). The proposed inventory substantially improves upon the existing national BDMOVES database, which is incomplete for this sector of the Pyrenees and aggregates multiple landslide types without specific kinematic information. Our RSF inventory is constructed through a combination of detailed geomorphological mapping and InSAR ground-motion data from the European Ground Motion Service (EGMS), complemented with press archives and reports provided by citizens and local institutions.

This new dataset enables a comprehensive assessment of the spatial and temporal distribution of RSFs, together with an in-depth analysis of their conditioning factors. In particular, we examine the role of lithology, slope aspect, and slope gradient, as well as the influence of debuttressing associated with post-glacial unloading, for each RSF type. The inventory also allows the construction of magnitude–frequency curves and the derivation of frequency–slope relationships, considering both the current slope gradients and those inferred for adjacent, unaffected slopes, which are used as a proxy for pre-failure topographic conditions. Altogether, these analyses facilitate the integration of RSFs into regional risk-management strategies and provide a robust baseline for comparison with analogous datasets from the Alps and the United Kingdom.

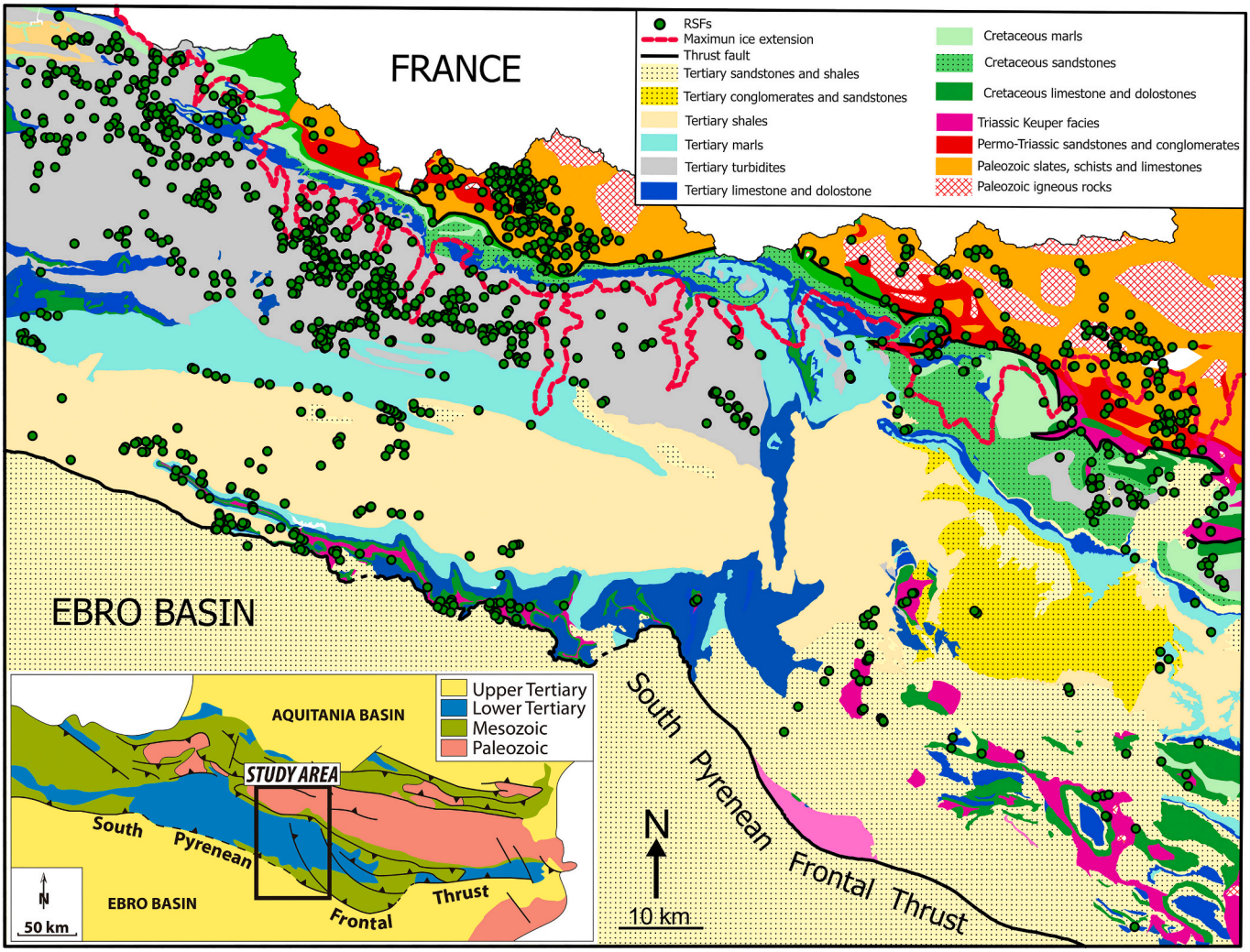


**Fig. 1.** Geological domains, main lithological units, thrust faults, maximum ice extension and spatial distribution of RSF (green dots) in the central Pyrenees.

## 2. Study area

The Pyrenees constitute a narrow, 70–120 km wide, 400 km long, alpine mountain range trending NNW–SSE that acts as a natural boundary between Spain, France, and Andorra (Fig. 1). This orogenic system developed in response to the convergence between the Iberian and European plates, spanning from the Late Cretaceous to the Miocene (Muñoz, 1992). From a structural standpoint, the range is relatively simple and is typically divided into three main tectonic domains (Barnolas and Pujalte, 2004). The core of the chain corresponds to the Axial Zone, composed mainly of exposed Paleozoic basement rocks. This unit is bordered to the north and south by fold-and-thrust belts formed by Mesozoic and Cenozoic sedimentary sequences, known respectively as the North-Pyrenean and South-Pyrenean Zones (Fig. 1). The South Pyrenean Frontal Thrust separates the Pyrenees from the Ebro Foreland Basin. The study area encompasses portions of both the Axial Zone and the central sector of the South-Pyrenean Zone (Fig. 1).

The Pyrenean Axial Zone is a segment of the European Variscan belt that was later reactivated and incorporated into the internal structure of the Pyrenees during the Alpine orogeny, from the Cretaceous to the Miocene (Matte, 1991). It comprises over 5000-m-thick, intensely deformed sequence of Paleozoic metasedimentary rocks, mostly slates, with subordinate schists, quartzites, and limestones, ranging in age from the Cambrian to the Carboniferous (Ríos et al., 1989; Barnolas and Pujalte, 2004). In the late Variscan stages, these rocks were intruded by calc-alkaline plutons (Santana Torre, 2002). Subsequently, E-W trending pull-apart basins developed along the southern margin of the Axial Zone and were filled with continental sediments and volcanic rocks (Rodríguez-Méndez et al., 2016). On the other hand, the South-Pyrenean Zone is a fold-and-thrust belt composed of Mesozoic to early Tertiary sedimentary rocks that were transported southward. The contact between the South-Pyrenean and Axial Zones is stratigraphic in the western sector, transitioning into a tectonic boundary marked by major thrust faults and significant structural complexity toward the east (Fig. 1). The stratigraphic sequence comprises Upper Triassic evaporites and mudrocks of the Keuper facies, followed by Cretaceous and Paleocene limestones, marls, and mudstones, and culminating in a thick, progradational Eocene succession. This latter sequence records a progressive transition from deep marine to shallow continental environments and includes turbiditic flysch, platform limestones, bluish marls, fluvio-deltaic deposits, and continental molasse (Gil et al., 2012; Montes, 2012).

From a geomorphological perspective, the maximum extent of glaciation during the Maximum Ice Extension (ca. 65 ka; Lewis et al., 2009; García-Ruiz et al., 2013) divides the central Pyrenees into two major domains. The northern domain includes most of the Axial Zone and the elevated limestone summits of the South-Pyrenean Zone, which underwent multiple glaciations throughout the Quaternary and are characterized by classic glacial landforms such as steep U-shaped valleys and sharp ridges. In contrast, the southern domain exhibits a predominantly fluvial landscape, locally covered by fluvial terraces and pediment deposits. The position of the terminal moraines from the MIE (red line in Fig. 1) marks the transition between these two geomorphic regions.

The climate of the Pyrenees is highly variable, with a pronounced North-South gradient in temperature and moisture conditioned by the altitude. The northern area with a higher relief and peaks exceeding 3000 m, is characterized by an Atlantic climate with mild temperatures and annual precipitation over 1500 mm/yr. The 0 °C isotherm is about 2700 m in elevation, and snowpack above 2000 m typically persists for six months (López-Moreno et al., 2020 and references therein). Southwards, as the altitude of the summits progressively decreases, the climate becomes warmer and drier with higher mean temperatures of 12 °C and annual precipitation as low as 650 mm (CHE, 2025).

## 3. Methodology

The geomorphological mapping of RSFs was performed manually using high-resolution orthoimages taken in 1956, 1978, 2003, 2006, 2009, 2012, 2015 and 2021 and a 5 m spatial resolution digital elevation model (DEM) downloaded from the Spanish Geographic Institute (IGN). All this information was integrated into a 3D ArcGIS Pro project providing multiple three-dimensional images of the same location at different years. The database was complemented with the review of local press archives, research papers, engineering reports and the BDMOVES national inventory of land movements (IGME, 2025). Each RSFs, which was recorded as a polygon feature, holds information regarding the typology, activity, velocity, lithology, damages and spatial and temporal data, following the guidelines of Guzzetti et al. (2012) and Valenzuela et al. (2017). The topographical and morphometric parameters (length, width, area, maximum and minimum altitude, slope, and aspect) were extracted from the DEM. In order to compare differences between pre-failure and post-failure slope conditions, the mean slope of the landslide bodies was measured and compared with that of the adjacent, undisturbed slopes, sampled 50 m from the landslide boundary and assumed to represent the pre-failure topography. Their spatial distribution with respect to lithology was analysed using the nearest neighbour index (R) to evaluate deviations from complete spatial randomness. The volume of RSFs was roughly estimated based on their surface area using a power law function:

$$V = k \times A^{\alpha}$$

where k is a constant and α is an exponent. Among the numerous empirical volume–area relationships proposed in the literature (Guthrie and Evans, 2004; Jaboyedoff et al., 2020, and references therein), the equations that best fit the only two landslides in the study area with known volumes, constrained by borehole and inclinometer data (Portalet earthflow, No. 28 in the inventory; Cobos et al., 2021 and Marmayor rock slide, No. 386; Pinyol et al., 2022 DiNSAR), are those of Guzzetti et al. (2009) for earthflows and He et al. (2023) for rock slides (Table 1). Based on a global compilation of landslide inventories, they derived scaling parameters of $k = 0.074$ and 0.27 and $\alpha = 1.45$ and 1.4 respectively. Other relationships (e.g. Guthrie and Evans, 2004; Imaizumi and Sidle, 2007; Jaboyedoff et al., 2020; Ju et al., 2023) tend to either underestimate or overestimate the landslide volume by projecting the failure surface as shallower or deeper, respectively. Based on comprehensive landslide inventories in Japan (Ogita et al., 2017) and the Himalayas (Xu et al., 2016; Zhao et al., 2019), and considering their estimated volumes, we define large-scale landslides as those involving downslope-moving masses exceeding $1 \times 10^6$ m$^3$.

The activity status of RSFs was determined from the European Ground Motion Service (EGMS) InSAR (Interferometric Synthetic Aperture Radar) dataset. The EGMS viewer provides open access to high-quality and consistent Line-Of-Sight (LOS) displacement maps from both ascending and descending satellite orbits, as well as their vertical (Vv) and horizontal (Vh) displacement components since 2016 to 2023 across Europe. The displacement measurements are derived from advanced DInSAR processing of full-resolution Sentinel-1 imagery, utilizing both Permanent Scatterers (PS) and Distributed Scatterers (DS) techniques. Fundamental aspects of the EGMS framework are detailed in the White Paper (EGMS, 2017), while the implementation strategy and product specifications are outlined in the official documentation (EGMS, 2020). Additionally, the technical methodologies underpinning EGMS have been comprehensively reviewed in Crosetto et al. (2021) and Ferretti et al. (2021).

RSFs were classified based on both typology and activity. Following the classification proposed by Jarman and Harrison (2019) and Blondeau et al. (2021), rock slope failures were initially categorized into rock avalanches, rock slides (including both translational and rotational types), and rock slope deformations (RSDs), also referred to as deep-

**Table 1**
Estimated volumes (in bold) of RSFs No. 28 (Cobos et al., 2021) and No. 386 (Pinyol et al., 2022), derived from borehole and inclinometer data as well as power-law functions within the study area. Values in bold red indicate the best fit with the volumes estimated from subsurface data.

| Landslide number | Volume from borehole and inclinometer data | Volume from power law functions | | | | |
|---|---|---|---|---|---|---|
| | | Imaizumi and Sidle (2007) | Guzzetti et al. (2009) | Jaboyedoff et al. (2020) | He et al. (2023) | Ju et al. (2023) |
| Portalet earthflow (No. 28) | **12.3** | 10.8 | **12.8** | 15.8 | 24.3 | 1.69 |
| Marmayor rock slide (No. 386) | **11.9** | 4.6 | 5.4 | 6.6 | **9.9** | 0.8 |

seated gravitational slope deformations (DSGSDs) in the literature (Crosta et al., 2013). However, this scheme did not encompass the full range of movement types identified in the study area, which is predominantly composed of fine-grained sedimentary and metamorphic rocks. To address this limitation, two additional categories were incorporated, based on the classifications of Varnes (1978) and Hungr et al. (2013): earthflows and composite failures. The term earthflow is defined within the landslide classification system as a flow-type, intermittent, mass movement typically occurring in fine-grained and deformable materials (Hungr et al., 2013). While originally applied to soil, similar flow-dominant behaviour can emerge in highly weathered, deformed or weak rock masses lacking intact structure, leading to mobilization with lobate tongue-like morphology (e.g., Schönfeldt et al., 2020). Given that most mobilized masses lack sufficient outcrops to assess internal deformation structures, the term *earthflow, preferred here over flowslide (*Hungr et al., 2013*),* is used here in a broad sense to describe rock masses that have undergone partial or complete disintegration and show a flow-type downslope movement and fan-shaped morphologies. *Composite failures* refer to slope movements involving a combination of two or more types of mass-wasting processes.

Finally, based on the available InSAR data derived from the EGMS and considering its detection threshold of 3 mm/yr under ideal PS/DS conditions (Crosetto et al., 2021; Ferretti et al., 2021), RSFs were categorized into three classes: active (InSAR displacement over 3 mm/yr showing coherent movement across most of the surface, fresh-looking appearance with undulated topography, cracks, depressions and lack of well-developed drainage), inactive (InSAR displacement less than 3 mm/yr and an incised drainage network) and unknown (no InSAR displacement data and mostly covered by a dense vegetation, which inhibits the observation of their surface topography). Nevertheless, several constraints limit the ability of InSAR-based approaches to identify RSFs and quantify their moving rates (e.g., Yi et al., 2023; Ciuffi et al., 2024). In particular, signal decorrelation is mainly driven by persistent snow cover, unfavourable north-facing slopes with low sensitivity to the satellite line of sight, geometric distortions, and topographic shadowing, which may result in active RSFs being classified as unknown.

## 4. Results

### 4.1. Morphometric analysis

A total of 1232 RSFs (Fig. 1) were identified within a study area of 11,443 km$^2$, resulting in an overall density of 0.11 RSF per km$^2$. Regarding the kinematic typology of the failures (Fig. 2), rotational rock slides are the most abundant type, comprising 746 events (60.5%), followed by earthflows with 309 cases (25.1%). Translational rock slides account for 102 events (8.3%), while RSDs ($n$ = 39), composite failures ($n$ = 29), and rock avalanches ($n$ = 7) are less frequent. In terms of activity, based on InSAR data, only 129 out of 1232 RSFs are considered active with very slow to extremely slow current average displacement velocities between 5 and 75 mm/yr, according to the velocity classification of Cruden and Varnes (1996). Earthflows exhibit the highest number of active processes ($n$ = 54), closely followed by rotational rock

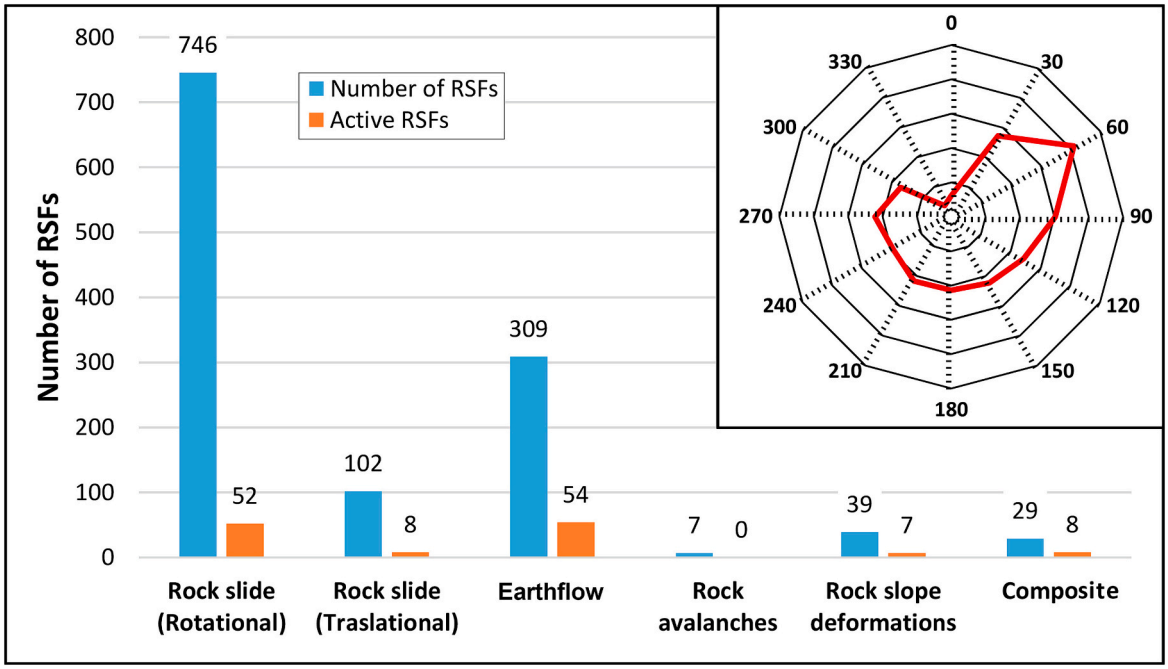


**Fig. 2.** Typology, activity and aspect of RSFs.

slides ($n = 52$). Limited activity was observed for translational slides ($n = 8$), slope deformations (n = 7), and composite types (n = 8), while no active rock avalanches were recorded. The data reveal a non-uniform distribution of RSFs across aspect classes, suggesting that slope orientation significantly influences failure susceptibility (Fig. 2). Notable trends include the highest concentration of RSFs between 30° and 90° (36.4%). These correspond to generally northeast to east-facing slopes. The lowest frequencies are observed between 330° and 30° (3.4%), indicating relatively north-facing aspects are less susceptible in this dataset. A relatively low even distribution is found between 120° and 300°.

The morphological and volumetric characteristics of the RSFs display substantial variability across failure types (Table 2). Composite landslides and RSDs show the largest average affected areas, with mean values of 1,049,727 $m^2$ and 974,468 $m^2$, respectively, and volumes averaging 59.1 $hm^3$ and 47.5 $hm^3$. In contrast, rock slides, although the most frequent, are significantly smaller in scale, with a mean area of 99,139 $m^2$ and an average volume of 2.1 $hm^3$. Rock avalanches and earthflows exhibit intermediate mean volumes of 7.7 $hm^3$ and 4.1 $hm^3$, respectively. With the exception of rock avalanches, which occur on subvertical to vertical slopes, the remaining types of RSFs predominantly develop on moderate slope gradients, generally ranging between 19° and 23°.

A clear association between RSF types and glacial conditioning is evident. A significant proportion of documented rock slope failures (RSFs) have occurred within glaciated environments, with a marked variability across failure types. Specifically, 87.5% of rock avalanches, 71.8% of RSDs, 72.4% of composite failures, and 61.8% of earthflows have been reported in previously glaciated settings. In comparison, only 20% of rock slides occurred within glaciated environments.

Furthermore, in general, failures tend to occur at increasingly higher altitudes and steeper slopes in the order: rock slides < earthflows < rock avalanches < composite < RSDs, suggesting a gradient of topographic control linked to failure complexity and scale.

The distribution of RSFs was analysed in relation to lithology across the study area (Fig. 3). In addition, its density was normalized by the outcropping area of each lithology, allowing for comparison independent of surface exposure. RSFs are predominantly concentrated in sedimentary rocks, particularly within turbidites, which exhibit the highest number of failures ($n = 623$), accounting for 50.7% of all RSFs, and showing the highest density (1.329 RSFs/$km^2$). Metamorphic rocks, mainly slates, represent the second most affected lithology, with 296 failures (24.1%) and a moderate density of 0.104 RSFs/$km^2$. Other sedimentary formations such as mudstones ($n = 112$; 9.1%), marls ($n = 83$; 6.8%), and evaporites ($n = 73$; 5.9%) also contribute significantly to the total RSFs, particularly evaporites, which show a density of 0.171 RSFs/$km^2$. In contrast, igneous rocks (andesites and granitoids) present the lowest susceptibility, with only 5 RSFs combined, representing less than 0.5% of the total events and showing negligible densities (< 0.003 RSFs/$km^2$).

Lithology significantly influences the type and frequency of RSFs due to inherent variations in the mechanical strength, porosity, permeability, friction angle, cohesion, and susceptibility to weathering (Fig. 4). Rock avalanches predominantly occur in conglomerates and limestones (80%), with a smaller contribution from igneous rocks (20%). These lithologies are typically strong and brittle, promoting sudden detachment and catastrophic failure when internal stresses exceed rock strength, particularly in fractured zones due to glacial debuttressing. Rock slides are most common in turbidites (60%), slates (12%), and mudrocks (10%). The layered and fissile nature of these rocks facilitates planar and rotational sliding along bedding planes or foliations. Low-strength units like Keuper facies and marls also contribute to reduced shear strength. Earthflows are dominated by slates (64%) and turbidites (25%), which become plastic and mobile when saturated. These rocks generally have high water retention and low shear resistance, ideal conditions for flow-type failures. Composite movements reflect the interaction of multiple lithologies: turbidites (38%), keuper facies (23%), marls (16%), and slates (15%). The variability in mechanical behaviour across these units leads to mixed-mode deformation combining sliding and flowing processes. Finally, RSDs occur primarily in *slates* and *turbidites* (both 45%), with minor contributions from *marls*. The layered structures and pervasive fracturing in these units permit deep-seated long-term deformation often manifesting as large-scale, slow moving gravitational creep.

### 4.2. Spatial distribution

The spatial distribution of RSFs was analysed using the nearest neighbour index (R) to assess deviations from complete spatial randomness in relation to underlying lithologies. Considering the total area, the observed mean nearest neighbour distance was 774.17 m, while the expected mean distance under complete spatial randomness was 1951.80 m. The resulting nearest neighbour index (R) was 0.397, indicating a clustered distribution pattern. Notably, RSF clusters are particularly concentrated in the eastern and western extremes of the study area (Fig. 1), where turbidites, slates, marls, and evaporites are exposed. However, when analysed by lithological unit, the R values were closer to 1: turbidites ($R = 0.86$), slates ($R = 0.94$), marls ($R = 1.13$), and evaporites ($R = 1.24$). These results suggest that the distribution of RSFs within individual lithologies tends to approximate randomness.

The cumulative area-frequency relationships for different landslide types exhibit distinct trends in the semi-logarithmic plot (Fig. 5). All four types show a negative logarithmic relationship. Rock slides (blue) follow a moderate negative trend with a strong correlation coefficient ($R^2 = 0.96$). This indicates a relatively balanced size distribution, where larger slope movements are less frequent but still present across a broad area range. Earthflows (red) show a slightly less steep trend and slightly displaced to the right, suggesting a greater proportion of medium to large bodies compared to rock slides. The distribution is still strongly logarithmic ($R^2 = 0.95$) but with a slower decay in frequency with increasing area. Composite movements (magenta) and RSDs exhibit the steepest trends with a sharp decline in frequency as area increases, although clearly displaced to higher values. This tendency predicts a dominance of large-scale movements in agreement with their typically massive extent and lower abundance. However, the number of composite movements and RSDs in the dataset is significantly lower than for other types. As a result, the data do not fit the logarithmic trend as precisely, and the reliability of the regression line is reduced despite their high $R^2$ values.

Additionally, the relationship between mean slope angle and cumulative frequency for different types of RSFs reveals distinct

**Table 2**
Mean morphometric parameters depending on the typology of the RSFs and number of RSF developed in glaciated areas.

| Typology | Area ($m^2$) | Volume ($hm^3$) | Altitude (masl) | Altitude difference (m) | Slope (°) | Number in glaciated areas | % in glaciated areas |
|---|---|---|---|---|---|---|---|
| Rock slide | 99,139 | 2.1 | 1100 | 129 | 22 | 170 out of 848 | 20.05 |
| Earthflow | 155,140 | 4.1 | 1517 | 179 | 19 | 191 out of 309 | 61.81 |
| Rock avalanche | 195,924 | 7.7 | 1267 | 280 | – | 7 out of 8 | 87.50 |
| Composite | 1,049,727 | 59.1 | 1654 | 419 | 23 | 21 out of 29 | 72.41 |
| RSD | 974,468 | 47.5 | 1728 | 440 | 27 | 28 out of 39 | 71.79 |

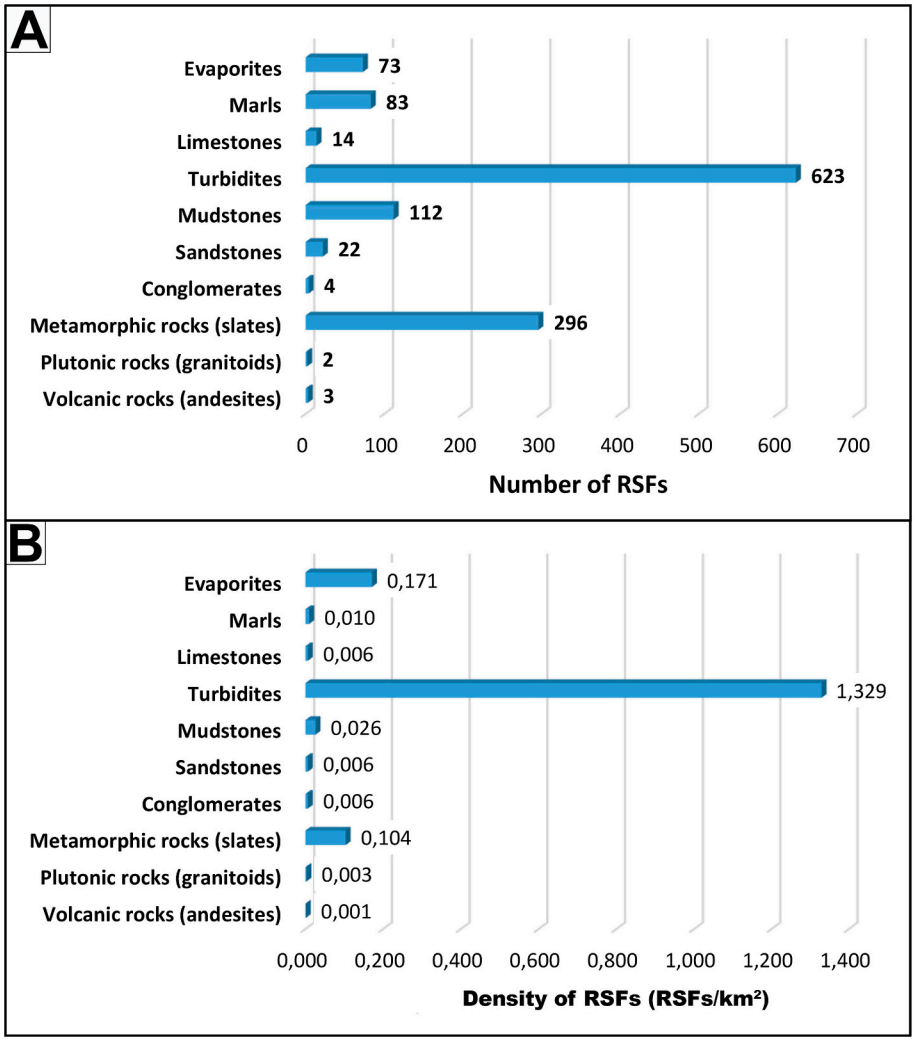


**Fig. 3.** Number and density of RSFs (RSFs/km$^2$) in relation to lithology.

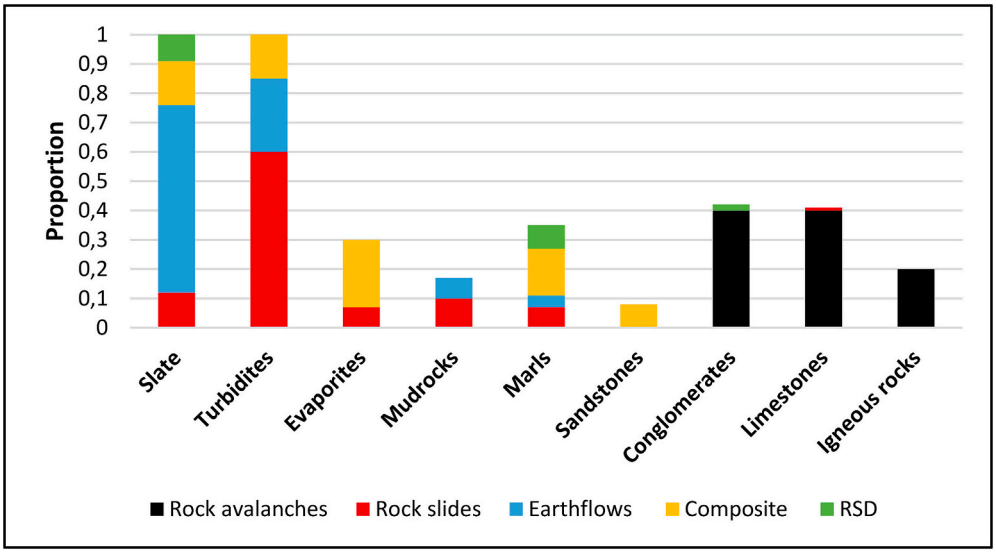


**Fig. 4.** Relationship between the typology of RSFs with the lithology.

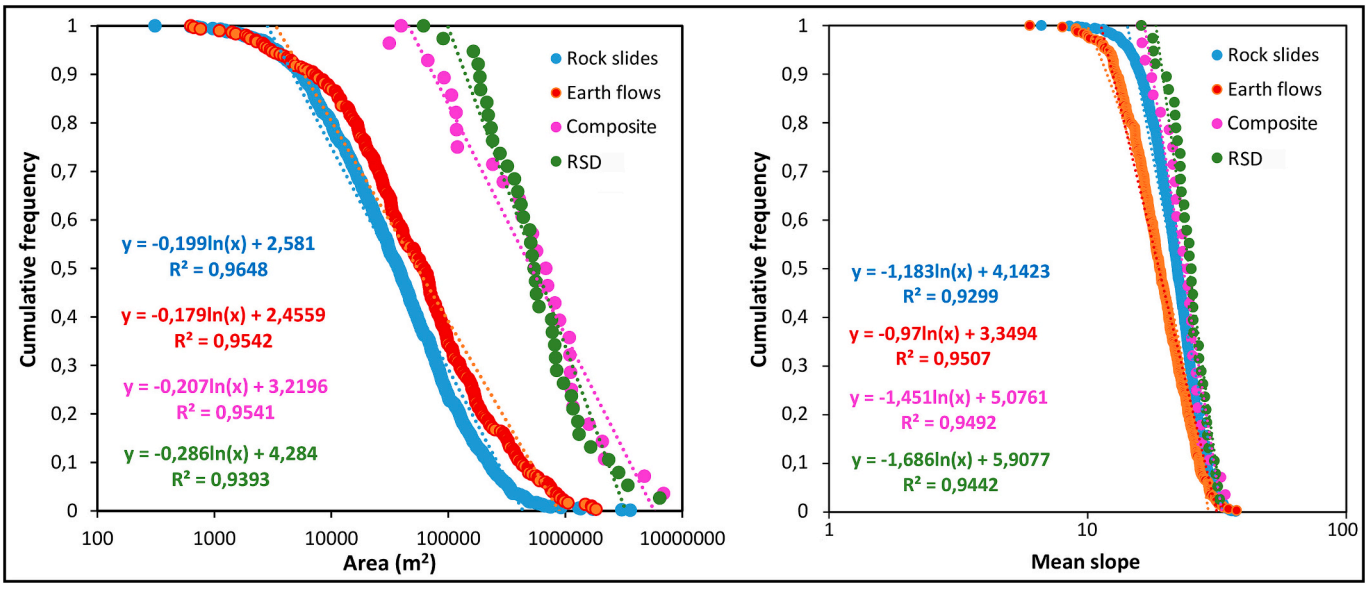


**Fig. 5.** Semi-log cumulative frequency plots showing cumulative frequency versus area and slope of the RSFs based on their typology, and best-fit regression functions (dotted lines).

behavioural trends across landslide mechanisms. All landslide types display a clear negative linear relationship between mean slope and cumulative frequency with a high coefficient correlation ($R^2 > 0.94$), suggesting that the likelihood of occurrence generally decreases as slope steepness increases. In general, most RSFs tend to occur on moderate slopes between 20 and 30 degrees. Rock slides and earthflows present gentler decline trends, with 90% of the population occurring at slopes of around 25°. Composite failures and RSDs exhibit steepest declines and

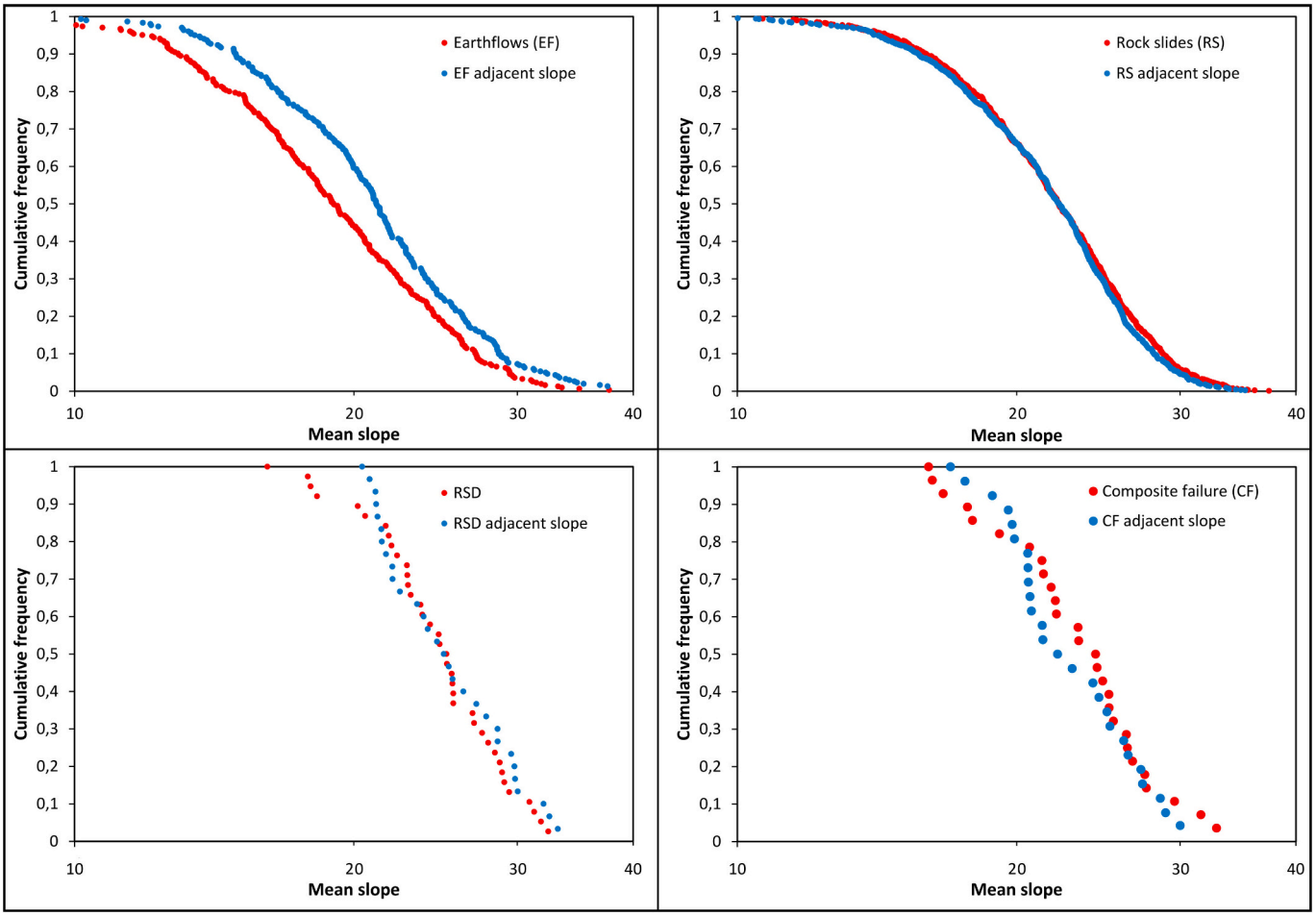


**Fig. 6.** Semi-log cumulative frequency plots showing cumulative frequency versus slope of the RSFs bodies and adjacent slopes based on their typology.

frequency curves displaced to higher slope values, indicating high concentration in steeper slopes compared to the other RSF types, often linked to large-scale, structurally controlled settings.

The comparison between the mean slope angle of landslide bodies and that of adjacent, undisturbed slopes (measured 50 m from the landslide boundary and assumed to represent pre-failure topography) reveals differences depending on the RSF typology (Fig. 6). Rock slides, composite failures, and RSDs exhibit highly similar cumulative frequency curves, indicating that their mean slope angles are broadly preserved relative to the original hillslope configuration. These types of failures typically involve limited internal deformation, approximately maintaining the overall mean inclination of the pre-failure slope. In contrast, the cumulative frequency plot for earthflows (Fig. 6 upper-left panel) reveals a distinct divergence between the slope-angle distributions of the failed bodies and their adjacent, undisturbed slopes. While both datasets exhibit a similar overall negative trend, the curve corresponding to the earthflow bodies is consistently displaced toward lower mean slope values of approximately 5°. This indicates that, following failure, the affected slopes experience a substantial reduction in gradient compared to the surrounding terrain, suggesting post-failure flattening of the surface. This behaviour reflects the rheological nature and kinematics of earthflows, which involve the progressive disintegration and fluid-like movement of fine-grained, brecciated bedrock downslope. During transport, the material tends to accumulate at lower elevations, producing a smoother and more gently inclined topography than the pre-failure slope.

### 4.3. Damage and threats associated with RSFs

RSFs exert substantial impacts on both natural environments and human infrastructure in the central Spanish Pyrenees. The vast majority of the RSFs occur in natural areas such as forests, grasslands, and agricultural fields. Despite their predominantly remote location, these RSFs induce significant environmental disruption by extensively altering slope morphology and drainage patterns. The headscarps of many rock slides and composite failures, as well as the back-tilted escarpments and split ridges typical of RSDs, frequently form elongated depressions that accumulate water and give rise to small lakes (Fig. 7A). Moreover, 70 RSFs have been documented to modify existing drainage networks. Among these, 48 RSFs, including 42 rock slides, 4 earthflows, 1 composite failure, and 1 RSD, have reached the bottom of the valley and caused partial or complete diversion of river channels running along their toes. These diversions lead to fluvial erosion on the opposite riverbank, promoting slope instability and triggering new both shallow and deep-seated landslides. Additionally, 25 landslide dams have been mapped across the study area, generated by 3 composite failures, 7 earthflows, 11 rock slides, and 4 rock avalanches (Fig. 7B). Notably, all mapped rock avalanches have resulted in full blockage of river courses.

Although most RSFs occur in natural landscapes, a significant proportion directly interacts with critical infrastructure, resulting in substantial socioeconomic consequences (Fig. 8; Table 1, supplementary material). According to the current inventory, dirt roads, typically used for rural or agricultural access, are the most affected, with 163 RSFs, although only 14 remain active. A total of 41 RSFs intersect pipelines, power lines, and irrigation networks, with 9 currently active events. The five ski resorts of the study area are particularly exposed, with 138 RSFs identified and 28 still active. Many ski slopes and chairlifts are located on landslide bodies, as RSFs generally exhibit gentler gradients, making them suitable for skiing. Although all are susceptible to RSFs, the Formigal ski resort, centrally located within the study domain, has experienced particularly severe consequences. RSFs there have led to the displacement of critical lift infrastructure and necessitated the


**Fig. 7.** A) 2.5 km-long and 90 m high head scarp composite RSF (No. 71) made up of three large bodies separated by the drainage network. B) La Inclusa rock avalanche (No. 1070) and associated infilled landslide dam.

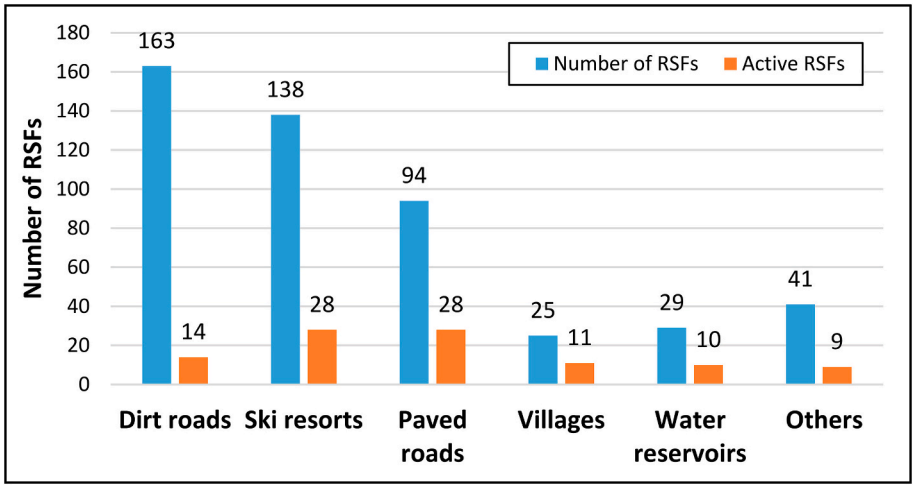


**Fig. 8.** Total and active RSFs affecting infrastructures. Pipelines, irrigation networks and power lines are included under Others.

abandonment and subsequent relocation of ski lifts. These events have incurred significant costs, including temporary service disruption and financial losses surpassing €5 million (Guerrero et al., 2018).

Paved roads are affected by 94 RSFs (rock slope failures), 28 of which are classified as active, posing a threat to connectivity and necessitating continuous maintenance or rerouting. The most affected transportation corridors are the A-23 highway and the A-136 transborder road, which constitutes one of the main trans-Pyrenean connections between Spain and France (Table 1, supplementary material). Along the A-23, between 2009 and 2018, three major slope movements necessitated repair and stabilization works exceeding €30 million. Along the A-136, a total of 18 large RSFs, 11 of them active, have caused damages exceeding €6.5 million and frequent traffic disruptions with unknown but significant indirect costs. The final 11-km stretch of this road demands ongoing repairs, including repaving, pile reinforcements, block retaining walls, and installation of drainage systems. From north to south, the Portalet (Fig. 9A), Furco (Fig. 9B), and Lanuza RSFs (no. 28, 26, and 12, respectively), with estimated volumes of 47, 118, and 46 $hm^3$ of disintegrated Devonian slates, are responsible for most of the damage. Based on satellite SAR data, GPS measurements, and inclinometer records, their current movement rates vary from 4 to 7 cm/year (Herrera et al., 2009, 2011, 2013; Cobos et al., 2021; Chen et al., 2025), causing


**Fig. 9.** Portalet (upper image) and Furco (lower image) RSFs affecting the A-136 road. Close-up views show damage to the Formigal ski resort parking lot and retaining structures.

road bulging and frequent repaving (Guerrero et al., 2018) with a total cost of €6.5 million (Table 1, supplementary material).

Twenty-five RSFs impact villages situated primarily at depressions located near the head or toe of the landslides. Eleven of these are currently active, posing ongoing hazards to residential zones. Among them, the Arguisal slide (Fig. 10B), measuring 3 km long, 1.4 km wide, and with a 2.9-km fresh scar, is the fourth largest RSF in the study area and the only one roughly investigated (García Ruiz et al., 2002; Lucia, 2015). According to these studies, rotated strata at the head, a bulging toe, and a sequence of ridges and linear depressions along the main body are characteristic of a deep-seated rotational slide (>100 m depth), primarily affecting Lower Eocene flysch formations. The landslide is displacing moraine deposits, overlying recent alluvial fan sediments, and altering both a lateral stream and the main river valley, posing a potential threat to two downstream villages (Lucia, 2015).

Water reservoirs are intersected by 29 RSFs, 10 of which are active and could potentially compromise dam safety. The most destructive and cost-damaging RSF is the Marmayor slide, which threatens the Yesa Reservoir (Fig. 10C and D). This 14 $hm^3$ landslide features a basal shear surface located 120 m deep at the interface between Eocene marls and flysch layers (Moya et al., 2022). Excavation works in 2012 to increase the storage capacity of the reservoir reactivated the slide (Gutiérrez, 2013), moving at a rate exceeding 3 cm/year (Gómez, 2018) and exerting pressure against the dam's right abutment (Esteban et al., 2022; Pinyol et al., 2022; INGEOTYC, 2023). In addition, this activity damaged the NA-2420 road, which was interrupted and repaired, and also caused severe damage to two residential areas that had to be evacuated, expropriated, and eventually demolished. Emergency mitigation measures included the removal of 1.6 $hm^3$ of material from the landslide head, construction of reinforced concrete retaining walls at the toe, installation of cable anchors for slope stabilization, and drainage systems (CHE, 2022). Based on official government publications reported by the media, the stabilization of the Yesa Reservoir's right slope has incurred a cost of approximately €111 million to date (Table 1, supplementary material). Considering that the original project budget was estimated at €113 million, the slope stabilization effort alone has nearly equalled the initial construction budget.

## 5. Discussion

### 5.1. Conditioning factors in RSF formation

The identification of the conditioning factors of RSFs is essential to apply suitable mitigation measures and to increase the predictive ability of landslide susceptibility models. According to Crozier (1986), conditioning factors, also known as influencing (Yang et al., 2024a, 2024b) or inherent factors (Liao et al., 2022), refer to features of the rock mass that make the slope susceptible to instability processes. These can be grouped into the following categories (eg: Guzzetti et al., 2012; Reichenbach et al., 2018): (1) Topographical factors mainly related with the slope, (2) Geological factors including lithology and structure, and (3) Geomorphological factors, such as river erosion and deglaciation.

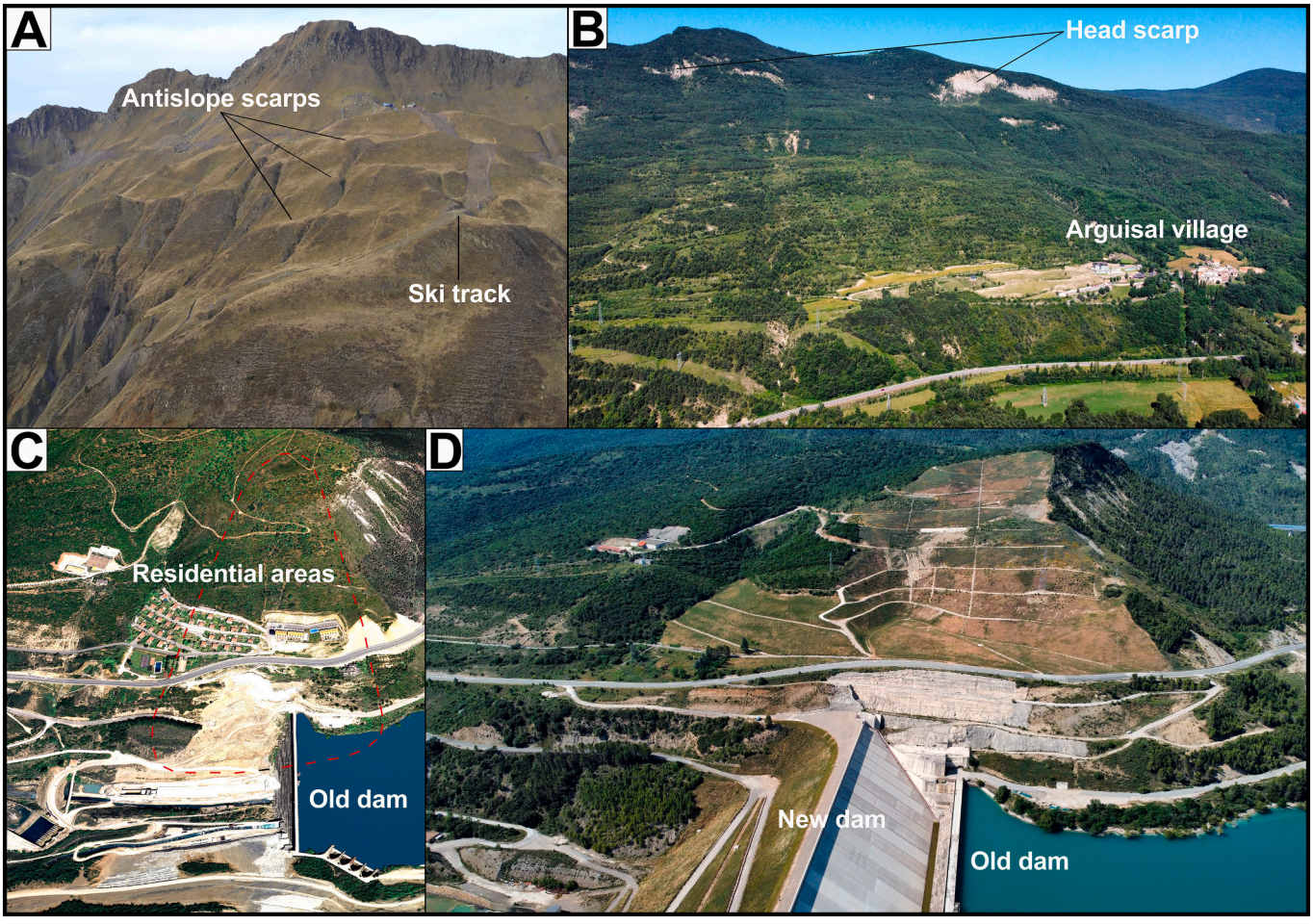


**Fig. 10.** A) Rock slope deformation (RSD) at the Astún ski resort (No. 74). Note the presence of multiple antislope scarps and the alignment of the ski track along the deformation zone. B) The Arguisal rotational rock slide (No. 327), characterized by a 2.6 km-long and 150 m-high head scarp, with the village located at the slide's toe. C and D) The Marmayor rock slide (No. 386), posing a threat to the Yesa Reservoir dams. The images show significant changes between 2011, prior to the excavation works, and 2025, highlighting the old and new dams, the demolished residential areas, and the slope stabilization measures implemented.

Slope and aspect are the main topographic factors that are always included in susceptibility studies by many researchers to understand landslide formation (eg: Capitani et al., 2013; Çellek, 2022). According to the latter author, more than 1500 research papers have used topographic factors in landslide susceptibility models and considers slope angle as the most influential and essential parameter in slope instability. In the Pyrenees, the slope-frequency curves emphasize the key role of slope angle in conditioning RSFs occurrence. Except for rock avalanches that are formed in subvertical scarps, the consistently moderate slopes observed in the cumulative frequency curves (Fig. 5) across most RSF categories point to a common geomorphological context characterized by moderate relief rather than extreme topographic gradients. 90% of the RSFs happen in slopes between 20 and 30° and less than 10% over 30° with none over 40°. These values are in agreement with other studies where it is reported that slopes ranging from 15° to 35° are more prone to instability processes (Lee and Min, 2001; Ercanoğlu et al., 2004; Hong et al., 2017; Pham et al., 2017) with a sharp drop in landslide intensity when slopes become steeper (Jaafari et al., 2015; Chen et al., 2018). Although, moderate slopes dominate overall landslide frequency, the degree of slope slightly varies by landslide type with composite failures and RSDs displaying a tendency to occur on steeper slopes compared to other types. Their higher incidence on steeper slopes probably suggest that their development may be more strongly influenced by structural or deep-seated instability mechanisms. The large volumes of rock affected by composite movements and RSDs with average values of 59.1 $hm^3$ and 47.5 $hm^3$, respectively, that exceed by up to 25 times earthflows and rock slides mean volumes, support downslope movement along deeper shear surfaces. On the other hand, from a susceptibility modelling perspective, the slope-cumulative frequency plots exhibit a close correspondence between the mean slope of rock slides, RSDs and composite failure bodies and that of the adjacent, presumably undisturbed slopes (Fig. 6). In contrast, earthflows exhibit a marked divergence from the adjacent slope due to their pronounced internal deformation. Consequently, the mean slope of earthflows bodies cannot be considered representative of the original pre-failure topography. This observation is relevant for susceptibility mapping and highlights the need for careful consideration of slope modification processes when using slope metrics to infer landslide susceptibility.

The aspect-based analysis demonstrates that slope orientation plays a significant role in controlling the spatial distribution of RSFs (Fig. 2). The increased concentration of failures on NE-facing slopes, minor in the SW and few in the north-south line, highlights the importance of the structural geological factors in slope instability. In the Pyrenees, folds, normal faults and thrust faults are mainly aligned NW-SE (Muñoz, 1992) leading to a sequence of ridges and valleys following the same orientation and consequently to either NE or SW facing slopes. The dominance of NE against SW facing slope failures might be related to a higher availability of water that promotes mechanical and chemical weathering, decreases effective weight on shear surfaces and consequently, enhances sliding.

Lithology plays a fundamental role in dictating the typology, behaviour, and hazard potential of RSFs (Figs. 1 and 3). Slope movements are predominantly concentrated in slates and mainly in sedimentary rocks, particularly within turbidites and marls. All these rocks show a dense network of discontinuity planes that favours the development of failures surfaces and make them exhibit low mechanical strengths (Bogaard et al., 2000). According to the stress-strain curves reported in the literature for different types of rocks (Selby, 1993; Waltham et al., 2005; Akdag et al., 2021; Jian et al., 2022; Yang et al., 2024a, 2024b), the compressive and tensile strength of these fine-grained rocks might be up to 10 times lower than hard, competent quartzites, limestones, cemented conglomerates and igneous rocks, what explains the preference for RSFs formation in these low mechanical strength rocks. In addition, their mechanical behaviour is largely dependent on their number and angle of their discontinuities (bedding planes, lamination and cleavage) and mainly the water content. For example, uniaxial and triaxial compression tests show that the change to an elastic–plastic (ductile) behaviour with increasing moisture content causing a notable drop in their compressive strength to almost half under saturated conditions (Yang et al., 2024a, 2024b). Other authors, have pointed their property to reach residual strength values under small strain due to the reorientation of their constituent particles favouring downslope creeping movements (Stark and Eid, 1994, Rouaiguia, 2010; Guerrero and Gutiérrez, 2017; Liu et al., 2024).

The evaporitic beds of the Keuper Formation represent a distinctive case. Despite occupying a limited area within the study zone, this lithology exhibits the second highest density of RSFs, with a total of 73 failures and a density of 0.17 slope movements per square kilometre (Fig. 3). In the central South Pyrenean sector, this lithostratigraphic unit consists of an alternation of gypsum layers, shales, and marls (Salvany and Bastida, 2004). While only gypsum is exposed at the surface, borehole data (Klimowitz and Torrescusa, 1990) and the presence of saline springs indicate halite deposits at depth (Pérez Bielsa et al., 2012; Rodríguez Gómez, 2015). The shales and marls are rich in clay minerals such as illite, chlorite, and interlayered chlorite–smectite clays (Salvany and Bastida, 2004). The weathering of this evaporite–clay assemblage, primarily driven by the dissolution of evaporitic beds and the swelling behaviour of clays, contributes significantly to slope instability. The dissolution of near-surface gypsum and deeper salt beds leads to the development of voids, progressive loss of rock structure, and a consequent reduction in shear strength parameters including cohesion and internal friction angle. Several studies (Guerrero and Gutiérrez, 2017; Migoń et al., 2023) have documented the role of evaporite karst in triggering landslides in both the Alps and the Ebro Basin. Additionally, the dissolution-widened fractures within evaporite layers facilitate the downward migration of water to underlying shales. These shales, due to their high content in illite and smectite, undergo significant volume increases, over 50% and up to fourfold, respectively (Ohazuruike and Lee, 2023), through mechanisms such as crystalline and osmotic swelling (Du et al., 2018). This hydration-driven expansion results in microfracturing, volumetric deformation, and a drastic decline in mechanical strength. Upon water infiltration, the affected clay-rich rocks may experience a sharp reduction in compressive strength and Young's modulus, ranging from 2- to 35-fold decreases, potentially leading to complete disintegration without the need for additional external forces, depending on the total clay content (Du et al., 2018; Shi et al., 2019; Chen et al., 2020, and references therein). These findings underscore the critical role of lithology, especially rock strength and weathering susceptibility, in promoting mechanical degradation of the rock mass and landslide development.

Finally, glacial debuttressing, which refers to the loss of lateral support following glacier retreat, is considered to be one of the most important geomorphological conditioning factors in slope instability (Ballantyne, 2002; Ballantyne et al., 2014a). The removal of confining pressure on valley walls induces stress-release fracturing and the uplift and dilation of the rock mass reducing rock strength and preconditioning slopes for failure (McColl, 2012; Ballantyne et al., 2014b). In the study area, the majority of rock avalanches, RSDs, composite failures and earthflows have occurred in glaciated terrains. This distribution highlights the strong geomorphic and mechanical influence of past glaciation and glacial unloading on slope stability. Unfortunately, there is a limited number of studies dealing with the age of RSFs in the Pyrenees. In glaciated areas, the radiocarbon dates of sediments trapped in antislope scarps in two RSDs located in the western sector of the study area yield ages between 5.6 and 7.8 cal ka while deglaciation of this sector occurred between 16 and 13 ka (Gutiérrez et al., 2005, 2008). In the eastern sector of the study area, Guerrero et al. (2018) studied 5 relict landslide dams related to the blockage of drainages by postglacial earthflows developed on Paleozoic slates in the Gallego valley. Radiocarbon and single-grain optically stimulated luminescence (OSL) ages obtained on the lake sediments were between 45 and 15 ka, while deglaciation occurred before 45 ka. Outside of the study area, in the

French axial Pyrenees, the 10Be terrestrial cosmogenic radionuclide surface exposure (CRE) dating of a DSGSDs head scarp provides an age of 1.3 ka coinciding with the time of the Lavender earthquake (Lebourg et al., 2014). In this sector, glacial moraines are older than 10 ka (Taillefer, 1969). These observations suggest that glacial erosion and the subsequent debuttressing had a preparatory influence in slope instability, but did not directly trigger RSFs. This in agreement with previous studies on the timing of rock slope failures using different dating techniques that evidence slope movement formation long after or throughout almost the entire postglacial period (eg: Soldati et al., 2004; Ballantyne et al., 2014a, 2014b; Dixon et al., 2024 and references therein).

### 5.2. Magnitude-frequency analysis

Although numerous landslide inventories have been developed to analyze magnitude–frequency relationships, most of them consider all types of slope movements, encompassing failures in soil, unconsolidated Quaternary deposits, and bedrock (Guzzetti et al., 2002; Guthrie and Evans, 2004; Guthrie et al., 2008; Tebbens, 2020), often triggered by individual rainfall (Samodra et al., 2020) or seismic events (Zhou et al., 2016). These datasets, while extensive, generally do not differentiate between material types or failure mechanisms. In contrast, to our knowledge, only two studies in the existing scientific literature have focused exclusively on RSFs. These are Jarman and Harrison (2019), based on an inventory of 1082 sites from the British mountains in the United Kingdom (UK), and Blondeau et al. (2021), based on a complete dataset of 1416 RSFs from the Western Alps.

The plot (Fig. 11) shows the cumulative frequency of RSFs as a function of their area (in $m^2$, log scale) across these two datasets and our study area in the Pyrenees (Fig. 10), allowing for a direct comparison of RSF-dominated regions across different tectonic and climatic contexts. Each dataset includes a logarithmic regression with its corresponding equation and $R^2$ value, indicating strong negative log-linear relationships between landslide area and cumulative frequency independently of the study area. However, the magnitude–frequency distributions highlight notable differences between the Pyrenees and other mountain regions. The red curve, representing all RSFs in the study area, exhibits a gentler slope, indicating a lower relative frequency of large-magnitude events and a greater proportion of smaller-scale failures. This contrasts with the steeper distributions from the UK and Alps, where large failures are more prevalent. Two main factors explain this deviation. Firstly, the study area shows a higher proportion of rock slides and earthflows, while RSDs are proportionally abundant in the UK and Alps datasets. This is probably due to the higher predominance of highly tectonized, mechanically weak, fine-grained lithologies (shales, marls, and slates) in the Pyrenees, which promotes the development of rock slides and their rapid transformation into earthflows. Secondly, the dataset of our study area explicitly includes earthflows, a landslide type that is absent in the UK and Alpine inventories, thereby increasing the number of small-area events and shifting the distribution accordingly. Interestingly, the pink curve, which isolates only composite RSFs and RSDs, is steeper than the total RSFs alone and shows a similar trend as the UK dataset and nearly identical to the Alps curve. This near-perfect match strongly supports the initial hypothesis that when rock slides and earthflows are excluded, the magnitude–frequency distribution in the study area aligns well with patterns observed in other mountainous regions and confirms the dominant influence of rock slides and earthflows on the distinct behaviour of the complete dataset in the Pyrenees.

### 5.3. Importance of inventories to prevent damages

Reducing landslide risk fundamentally depends on comprehensive inventories. Key articles, such as those by Guzzetti et al. (1999, 2012), Hervás and Bobrowsky (2009), Hervás (2013), underscore that inventories are crucial for understanding the distribution and recurrence of these phenomena. They form the cornerstone for developing accurate susceptibility, hazard, and risk maps (Van Westen et al., 2006; Fang et al., 2024). Without a detailed record of historical landslides, risk assessment remains incomplete, thereby limiting the effectiveness of mitigation measures and land-use planning.

Prior to this study, the BDMOVES inventory, developed by the Geological Survey of Spain (IGME, 2025), constituted the most comprehensive landslide database in the central Spanish Pyrenees, identifying a total of 123 RSFs. The new inventory includes 1232 RSFs, representing an increase of over 1000 failures and an approximate 1000% growth in the number of mapped events. This updated inventory provides critical insights into the long-term impacts of RSFs on both the natural landscape and human infrastructure information that was previously lacking. Although most of RSFs occur in natural landscapes

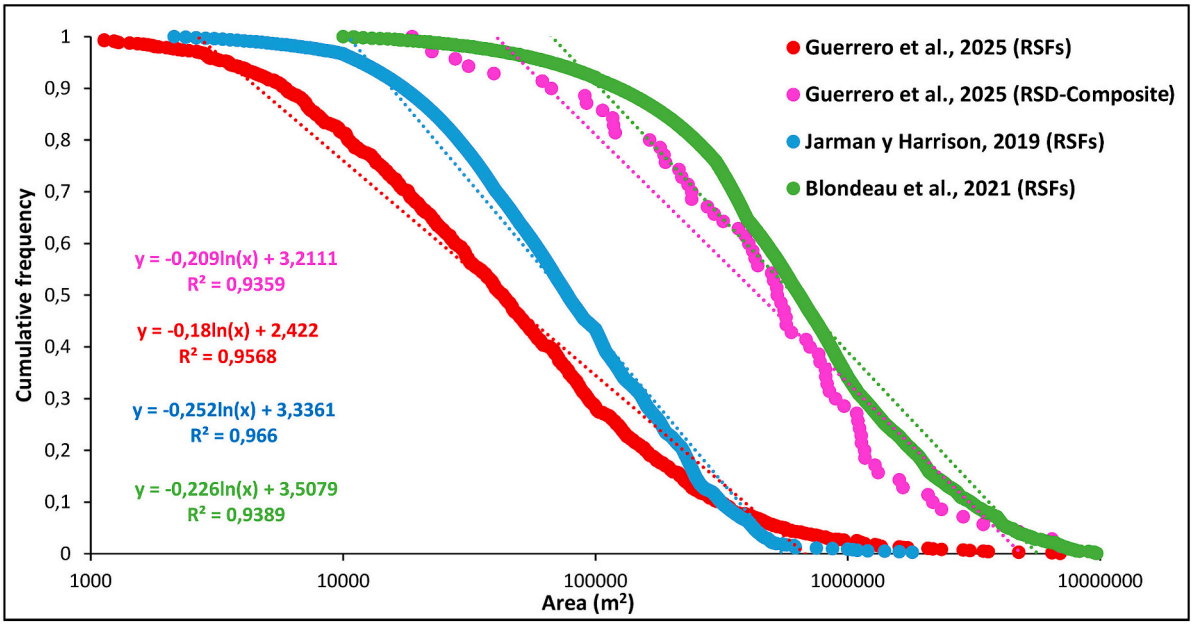


**Fig. 11.** Cumulative frequency–area distributions of RSFs from the study area and different mountain regions.

reshaping landscapes and disrupting hydrological systems, a significant proportion directly interacts with critical infrastructure, resulting in substantial socioeconomic consequences (Fig. 8). Historically, human settlements in mountainous areas have been strategically located in relatively flat, well-oriented, and sheltered terrain. Ironically, these flatter areas frequently correspond to ancient landslide deposits, where mass movement has significantly reduced slope gradients. In the absence of historical awareness of past slope failures, many villages have been built directly on these deposits. In the 1940s, the Salinas de Jaca rockslide caused severe damage and led to the abandonment of the town (Gutiérrez et al., 2014). Currently, 25 settlements are affected by RSFs, with 8 of these being particularly threatened due to their location within active movements. These communities will require multimillion-euro investments to stop movement.

The old, unwitting construction of villages on unstable slopes contrasts with recent infrastructure developments such as ski resorts, paved roads, high-voltage lines, and reservoirs, which often intersect RSFs that could have been avoided through proper geohazard assessment and use of detailed landslide inventories. The economic consequences of RSFs in the study area are already substantial and are expected to increase due to continued infrastructure development and the activation or reactivation of unstable slopes. Direct costs include structural damage to roads and infrastructure networks, rerouting or reinforcement of transport corridors, and emergency stabilization measures. For example, over €6.5 million has been spent on mitigation of RSFs along the A-136 road, over €5 million on ski lifts relocation and a minimum of €111 million has been allocated to stabilize the right slope of the Yesa Reservoir, nearly matching the original construction budget. In addition to these direct expenditures, indirect costs such as service disruptions, loss of tourism revenue due to ski resort closures and traffic interruptions, and forced evacuations of residential zones, further emphasize the economic burden of RSFs. This evidence underscores the vital importance of detailed, region-specific landslide inventories that distinguish between types of mass movements, their geomorphological behaviour, and interaction with anthropogenic structures. Ultimately, the development and maintenance of this robust RSF inventory will substantially reduce the long-term economic costs associated with slope instability in the Pyrenees providing essential tools for land-use planning, engineering design, and emergency response.

## 6. Conclusions

A total of 1232 Rock Slope Failures (RSFs) were mapped within the 11,443 $km^2$ study area, indicating a moderate density of 0.11 RSFs/$km^2$. Rotational rock slides are the most prevalent failure type, followed by earthflows and translational slides, whereas composite failures, RSDs, and rock avalanches are significantly less frequent. Despite the predominance of inactive processes, 129 RSFs (10.5%) are currently active, predominantly involving earthflows and rotational slides. Morphologically, the largest failures are associated with composite types and RSDs, while rotational and translational slides tend to be smaller in both area and volume.

The RSF inventory indicates that slope gradient, glacial debuttressing, and lithology exert strong controls on both the spatial distribution and typology of failures. Although most RSFs occur on moderate slopes (20–30°), slope–cumulative frequency analyses show that the mean slope angles of earthflows diverge markedly from those of adjacent, undisturbed slopes due to intense internal deformation. As a result, their mean slope cannot be considered representative of the pre-failure topography. This finding has important implications for susceptibility mapping, emphasizing the need to account for post-failure slope modification when interpreting slope metrics. The pronounced clustering of RSFs within formerly glaciated landscapes underscores the dominant role of glacial unloading, which induces fracturing and dilation, weakens rock masses, and enhances slope instability. This process is particularly significant in fine-grained, low-strength lithologies such as turbidites, marls, and slates, where mechanical weakness and pervasive discontinuities (e.g., bedding, foliation, cleavage) strongly favour failure. The evaporite- and clay-rich units of the Keuper Formation constitute a distinct case owing to their high susceptibility to subsurface dissolution, cavity development, and weakening of clays and marls, which swell and disintegrate upon hydration. The combination of mechanical fragility, swelling-prone clays, and evaporite karst processes produces highly unstable conditions even under minimal external forcing.

The cumulative area–frequency analysis of different RSF types in the Pyrenees reveals strong log-linear patterns in comparison with other mountain regions. However, the Pyrenean dataset exhibits a gentler slope, reflecting a dominance of smaller-scale failures. This deviation is explained by the higher relative frequency of rock slides and the explicit inclusion of earthflows in the inventory. Notably, when the Pyrenean dataset is limited to composite RSFs and RSDs, the resulting curve nearly mirrors other RSF magnitude-frequency studies, reinforcing that these large-scale failure types exhibit consistent magnitude–frequency behaviour across mountain belts.

Rock Slope Failures (RSFs) exert a substantial impact on infrastructures in the central Spanish Pyrenees with important economic consequences, resulting in over €152 million in direct damages in the last 20 years (more than €7.6 million per year in average). Despite the costly stabilization works that have included earthworks, flexible retaining walls and drainage installations, infrastructures need continuous maintenance. The interaction of RSFs with settlements presents additional concerns. Twenty-five towns and villages are built in areas directly affected by RSFs, 11 of which remain active. The tendency for human settlements to occupy topographic depressions, often formed by past deep-seated movements without recognition of the hazard, exposes communities to future reactivation and results in chronic vulnerability. These cases clearly illustrate the usefulness of comprehensive inventories for land-use planning to reduce RSF costs by avoiding susceptible areas, preventing RSF reactivation, estimating potential damage and designing more cost-effective interventions.

## CRediT authorship contribution statement

**J. Guerrero:** Writing – review & editing, Writing – original draft, Methodology, Investigation, Funding acquisition, Formal analysis, Data curation. **M. Guerra:** Writing – review & editing, Methodology, Investigation. **G. Desir:** Writing – review & editing, Investigation. **A. Serreta:** Writing – review & editing, Validation, Methodology. **Y. Thiery:** Writing – review & editing, Validation, Supervision, Investigation. **P. Lucha:** Writing – review & editing, Validation, Methodology.

## Funding

This research has been supported by the Government of Aragon (E02/23R) and the European Union Interreg VI-A España-Francia-Andorra (Poctefa 2021–2027), project SPIRAL EFA039/01. M.G. has a research contract financed by the European Union.

## Declaration of competing interest

The authors declare that they have no known competing financial interests or personal relationships that could have appeared to influence the work reported in this paper.

## Appendix A. Supplementary data

Supplementary data to this article can be found online at https://doi.org/10.1016/j.geomorph.2026.110172.

## Data availability

Data will be made available on request.

## References


Akdag, S., Karakus, M., Nguyen, G.D., Taheri, A., Bruning, T., 2021. Evaluation of the propensity of strain burst in brittle granite based on post-peak energy analysis. Underground Space 6, 1–11. https://doi.org/10.1016/j.undsp.2019.08.002.

Aparicio Valls, V., Ayala Carcedo, F.J., Sanz Pérez, E., 1987. Análisis del deslizamiento en Inza (Navarra) de 1714-15. Bol. Geol. Min. 98 (3), 112–122.

Ballantyne, C.K., 2002. Paraglacial geomorphology. Quat. Sci. Rev. 21, 1935–2017. https://doi.org/10.1016/S0277-3791(02)00005-7.

Ballantyne, C.K., Sandeman, G.F., Stone, J.O., Wilson, P., 2014a. Rock-slope failure following Late Pleistocene deglaciation on tectonically stable mountainous terrain. Quat. Sci. Rev. 86, 144–157. https://doi.org/10.1016/j.quascirev.2013.12.021.

Ballantyne, C.K., Wilson, P., Gheorghiu, D., Rodes, A., 2014b. Enhanced rock-slope failure following ice-sheet deglaciation: timing and causes. Earth Surf. Process. Landf. 39, 900–913. https://doi.org/10.1002/esp.3495.

Barnolas, A., Pujalte, V., 2004. La Cordillera Pirenaica. In: Vera, J.A. (Ed.), Geología de España. SGE-IGME, Madrid, pp. 233–241.

Blondeau, S., Gunnell, Y., Jarman, D., 2021. Rock slope failure in the Western Alps: a first comprehensive inventory and spatial analysis. Geomorphology 380, 107622. https://doi.org/10.1016/j.geomorph.2021.107622.

Bogaard, T.A., Antoine, P., Desvareux, P., Giraud, A., van Asch, Th.W., 2000. The slope movements within the Mondorès graben (Drôme, France), the interaction between geology, hydrology and typology. Eng. Geol. 55, 297–312. https://doi.org/10.1016/S0013-7952(99)00084-8.

Capitani, M., Ribolini, A., Bini, M., 2013. The slope aspect: a predisposing factor for landsliding? Compt. Rendus Geosci. 345, 427–438. https://doi.org/10.1016/j.crte.2013.11.002.

CHE, 2022. Informe del comportamiento de la ladera derecha de la presa de Yesa (Navarra), Febrero de 2022. Ministerio para la Transición Ecológica y el Reto Demográfico. Available in. https://portal.chebro.es/informe-de-la-presa-y-ladera-de-yesa (Accessed on 25 May, 2025).

CHE, 2025. SAIH Ebro, datos en tiempo real, estaciones meteorológicas. Disponible en. https://www.saihebro.com/tiempo-real/mapa-aforos-H5-gallego (accessed on 25 May, 2025).

Chen, W., Pourghasemi, H.R., Kornejady, A., Xie, X., 2018. GIS-based landslide susceptibility evaluation using certainty factor and index of entropy ensembled with alternating decision tree models. In: Pourghasemi, H., Rossi, M. (Eds.), Natural Hazards GIS-Based Spatial Modeling Using Data Mining Techniques, Advances in Natural and Technological Hazards Research, 48, p. 2018.

Chen, X., Yi, H., Gao, L., Shi, X., Liu, Y., 2020. Effects of inhibitor KCl on hydration swelling and softening of a smectite-poor mudstone. J. Pet. Explor. Prod. Technol. 10, 2685–2692. https://doi.org/10.1007/s13202-020-00948-8.

Chen, H., Zhao, C., Tomas, R., Reyes-Carmona, C., Kang, Y., 2025. Integrating InSAR and non-rigid optical pixel offsets to explore the kinematic behaviors of the Lanuza complex landslide. Remote Sens. Environ. 320, 114651. https://doi.org/10.1016/j.rse.2025.114651.

Ciuffi, P., Bayer, B., Berti, M., Franceschini, S., Simoni, A., 2024. InSAR stacking to detect active landslides and investigate their relation to rainfalls in the Northern Apennines of Italy. Geomorphology 457, 109242. https://doi.org/10.1016/j.geomorph.2024.109242.

Cobos, G., Eguibar, M.A., Torrijo, F.J., Garzón-Roca, J., 2021. A case study of a large unstable mass stabilization: "El Portalet" pass at the central Spanish Pyrenees. Appl. Sci. 11, 7176. https://doi.org/10.3390/app11167176.

Corominas, J., 2006. El clima y sus consecuencias sobre la actividad de los movimientos de ladera en España. Cuaternario Geomorfol. 20, 89–113.

Corominas, J., Lantada, N., Núñez-Andrés, M.A., Mavrouli, O.C., 2025. Fatal non-seismic rockfalls in Spain. Geoenviron. Disasters 12, 17. https://doi.org/10.1186/s40677-025-00317-9.

Crosetto, M., Solari, L., Balasis-Levinsen, J., Bateson, L., Casagli, N., Frei, M., Oyen, A., Moldestad, D.A., Mróz, M., 2021. Deformation monitoring at European Scale: the Copernicus Ground Motion Service. Int. Arch. Photogramm. Remote. Sens. Spat. Inf. Sci. XLIII-B3-2021, 141–146. https://doi.org/10.5194/isprs-archives-XLIII-B3-2021-141-2021.

Crosta, G., Frattini, P., Agliardi, F., 2013. Deep seated gravitational slope deformations in the European Alps. Tectonophysics 605, 13–33. https://doi.org/10.1016/j.tecto.2013.04.028.

Crozier, 1986. Field assessment of slope instability. In: Brunsden, D., Prior, D.B. (Eds.), Slope Instability. John Wiley and Sons Ltd., Chichester, UK, pp. 103–142.

Cruden, D.M., Varnes, D.J., 1996. Landslide types and processes. In: Turner, A.K., Schuster, R.L. (Eds.), Landslides. Investigation and Mitigation. National Academy Press, Washington, D.C., pp. 36–73

Dixon, J.L., Nicholas, G.E., Pierce, K.L., Lageson, D., 2024. Morphology, timing, and drivers of post-glacial landslides in the northern Yellowstone region. Earth Surf. Process. Landf. 49, 3873–3888. https://doi.org/10.1002/esp.5943.

Du, J., Hu, L., Meegoda, J.N., Zhang, G., 2018. Shale softening: observations, phenomenological behavior, and mechanisms. Appl. Clay Sci. 161, 290–300. https://doi.org/10.1016/j.clay.2018.04.033.

EGMS, 2017. White Paper. Available in. https://land.copernicus.eu/en/products/european-ground-motion-service/d2_d3_combined_sip_psd-1_01_final-1.pdf/@@download/file. (Accessed 14 May 2025).

EGMS, 2020. EGMS Implementation Plan and Product Specification Document. https://land.copernicus.eu/user-corner/technical-library/egms-white-paper (accessed 14 May 2025).

Çellek, S., 2022. Effect of the slope angle and its classification on landslides. Himal. Geol. 43, 85–95. https://doi.org/10.5194/nhess-2020-87.

Ercanoğlu, M., Gökceoğlu, C., Van Asch, Th.W.J., 2004. Landslide susceptibility zoning north of Yenice (NW Turkey) by multivariate statistical techniques. Nat. Hazards 32 (1–23), 2004. https://doi.org/10.1023/B:NHAZ.0000026786.85589.4a.

Esteban, F., Merino, M., Romero-Iribas, F., Lechón, A., 2022. Estabilización de la Ladera del Estribo Derecho de la Presa de Yesa (Navarra). X Simposio Nacional sobre Taludes y Laderas Inestables, SEMR, Granada, pp. 1–10.

Fang, Z., Wang, Y., van Westen, C., Lombardo, L., 2024. Landslide hazard spatiotemporal prediction based on data-driven models: estimating where, when and how large landslide may be. Int. J. Appl. Earth Obs. Geoinf. 126, 103631. https://doi.org/10.1016/j.jag.2023.103631.

Ferretti, A., Passera, E., Capes, R., 2021. Algorithm Theoretical Basis Document. EGMS Documentation. https://land.copernicus.eu/user-corner/technical-library/egms-algorithm-theoretical-basis-document (accessed 1 March 2025).

Froude, M., Petley, D., 2018. Global fatal landslide occurrence from 2004 to 2016. Nat. Hazards Earth Syst. Sci. 18 (8), 2161–2181. https://doi.org/10.5194/nhess-18-2161-2018.

García Ruiz, J.M., Lorente, A., González, P., Valero, B., Martí Bono, C., Segueria, S., 2002. El MegaSlump de Biescas-Arguisal, Pirineo Central, y su posible contexto temporal. In: Pérez González, A., Vargas, J., Machado, M.J. (Eds.), Aportaciones a la geomorfología de España en el Inicio del Tercer Milenio. Instituto Geológico y Minero de España, pp. 507–515.

García-Ruiz, J.M., Martí-Bono, C., Peña-Monné, J.L., Sancho, C., Rhodes, E.J., Valero-Garcés, B.L., González-Sampériz, P., Moreno, A., 2013. Glacial and fluvial deposits in the Aragón Valley, central-western Pyrenees: chronology of the Pyrenean late Pleistocene glaciers. Geogr. Ann. Ser. A, Phys. Geogr. 95, 15–32. https://doi.org/10.1111/j.1468-0459.2012.00478.x.

Gil, I., Barnolas, A., Montes, J., García-Ruiz, J.M., Peña, J.L., Bono, C., Gómez, A., 2012. Mapa Geológico de España 1:50.000, Sabiñanigo. IGME, Madrid, 83 pp.

Gómez, R., 2018. La Presa de Yesa. XVI Jornada Técnica Anual: casos singulares en la mecánica de rocas. In: Sociedad Española de Mecánica de Rocas (SEMR). Madrid, 25 de abril de 2018, 20 pp.

Guerrero, J., Gutiérrez, F., 2017. Gypsum scarps and asymmetric fluvial valleys in evaporitic terrains. The role of river migration, landslides, karstification and lithology (Ebro River, NE Spain). Geomorphology 297, 137–152. https://doi.org/10.1016/j.geomorph.2017.09.018.

Guerrero, J., Gutiérrez, F., García-Ruiz, J.M., Carbonel, D., Lucha, P., Arnold, L., 2018. Landslide-dam paleolakes in the Central Pyrenees, Upper Gállego River Valley, NE Spain: timing and relationship with deglaciation. Landslides 15. https://doi.org/10.1007/s10346-018-1018-9.

Guthrie, R.H., Evans, S.G., 2004. Analysis of landslide frequencies and characteristics in a natural system, coastal British Columbia. Earth Surf. Process. Landf. 29, 1321–1339. https://doi.org/10.1002/esp.1095.

Guthrie, R., Deadman, P., Cabrera, R., Evans, S., 2008. Exploring the magnitude-frequency distribution: a cellular automata model for landslides. Landslides 5, 151–159. https://doi.org/10.1007/s10346-007-0104-1.

Gutiérrez, F., 2013. Análisis geomorfológico de la ladera derecha de la Presa de Yesa (Río Aragón, Pirineos). Informe técnico. Universidad de Zaragoza, p. 27.

Gutiérrez, F., Acosta, E., Santiago, R., Guerrero, J., Lucha, P., 2005. Geomorphology and geochronology of sackung features (uphill-facing scarps) in the Central Spanish Pyrenees. Geomorphology 69, 298–314. https://doi.org/10.1016/j.geomorph.2005.01.012.

Gutiérrez, F., Ortuño, M., Pedro, L., Guerrero, J., Acosta, E., Coratza, P., Piacentini, D., Soldati, M., 2008. Late Quaternary episodic displacement on a sackung scarp in the Central Spanish Pyrenees. Secondary paleoseismic evidence? Geodin. Acta 21 (4), 187–202. https://doi.org/10.3166/ga.21.187-202.

Gutiérrez, F., Gutiérrez, M., Martín-Serrano, A., 2014. The geology and geomorphology of Spain, a concise introduction. In: Gutiérrez, F., Gutiérrez, M. (Eds.), Landscapes and Landforms of Spain. World Geomorphological Landscapes, Springer Science + Business Media, Dordrecht. https://doi.org/10.1007/978-94-017-8628-7_1.

Guzzetti, F., Carrara, A., Cardinali, M., Reichenbach, P., 1999. Landslide hazard evaluation: a review of current techniques and a complete geomorphological approach. Geomorphology 31, 181–216. https://doi.org/10.1016/S0169-555X(99)00078-1.

Guzzetti, F., Malamud, B.D., Turcotte, D.L., Reichenbach, P., 2002. Power-law correlations of landslide areas in Central Italy. Earth Planet. Sci. Lett. 195, 169–183. https://doi.org/10.1016/S0012-821X(01)00589-1.

Guzzetti, F., Ardizzone, F., Cardinali, M., Rossi, M., Valigi, D., 2009. Landslide volumes and landslide mobilization rates in Umbria, Central Italy. Earth Planet. Sci. Lett. 279, 222–229. https://doi.org/10.1016/j.epsl.2009.01.005.

Guzzetti, F., Mondini, A.C., Cardinali, M., Fiorucci, F., Santangelo, M., Chang, K.T., 2012. Landslide inventory maps: new tools for an old problem. Earth Sci. Rev. 112, 42–66. https://doi.org/10.1016/j.earscirev.2012.02.001.

Haque, U., Blum, P., da Silva, A., Andersen, P., Pilz, J., Chalov, S., Malet, J.P., Jemec, A., Andres, N., Poyiadji, E., Lamas, P., Wenyi, Z., Peshevski, I., Pétursson, H., Kurt, T., Dobrev, N., López-Davalillo, J., Halkia, M., Ferri, S., Keellings, D., 2016. Fatal landslides in Europe. Landslides. https://doi.org/10.1007/s10346-016-0689-3.

He, Y., Yu, J., Yuan, R., Nikitas, N., 2023. 3D modeling-based area-volume power-law relationships for incipient rotational slides. Geomorphology 441, 108885. https://doi.org/10.1016/j.geomorph.2023.108885.

Herrera, G., Fern'andez-Merodo, J.A., Mulas, J., Pastor, M., Luzi, G., Monserrat, O., 2009. A landslide forecasting model using ground based SAR data: the Portalet case study. Eng. Geol. 105, 220–230. https://doi.org/10.1016/j.enggeo.2009.02.009.
Herrera, G., Notti, D., García-Davalillo, J.C., Mora, O., Cooksley, G., S'anchez, M., Arnaud, A., Crosetto, M., 2011. Analysis with C- and X-band satellite SAR data of the Portalet landslide area. Landslides 8, 195–206. https://doi.org/10.1007/s10346-010-0239-3.
Herrera, G., Gutiérrez, F., García-Davalillo, J.C., Guerrero, J., Notti, D., Galve, J.P., Fern'andez-Merodo, J.A., Cooksley, G., 2013. Multi-sensor advanced DInSAR monitoring of very slow landslides: the Tena Valley case study (central Spanish Pyrenees). Remote Sens. Environ. 128, 31–43. https://doi.org/10.1016/j.rse.2012.09.020.
Hervás, J., 2013. Landslide inventory. In: Bobrowsky, P.T. (Ed.), Encyclopedia of Natural Hazards. Springer, Berlin, pp. 610–611.
Hervás, J., Bobrowsky, P., 2009. Mapping: inventories, susceptibility, hazard and risk. In: Sassa, K., Canuti, P. (Eds.), Landslides – Disaster Risk Reduction. Springer, Berlin, Heidelberg. https://doi.org/10.1007/978-3-540-69970-5_19.
Hong, H., Ilia, I., Tsangaratos, P., Chen, W., Xu, C., 2017. A hybrid fuzzy weight of evidence method in landslide susceptibility analysis on the Wuyuan area, China. Geomorphology 290, 1–16. https://doi.org/10.1016/j.geomorph.2017.04.002.
Hungr, O., Leroueil, S., Picarelli, L., 2013. The Varnes classification of landslide types, an update. Landslides 11, 167–194. https://doi.org/10.1007/s10346-013-0436-y.
IGME, 2025. Base de Datos de Movimientos del terreno (BDMOVES). Available in. https://info.igme.es/catalogo/resource.aspx?portal=1&catalog=3&ctt=1&lang=spa&dlang=eng&llt=dropdown&master=infoigme&resource=8308 (accessed on 25 May, 2025).
Imaizumi, F., Sidle, R.C., 2007. Linkage of sediment supply and transport processes in Miyagawa Dam catchment, Japan. J. Geophys. Res. Earth Surf. 112, 1–17. https://doi.org/10.1029/2006JF000.
INGEOTYC, 2023. Valoración del dictamen final sobre la seguridad de las obras del recremiento de la presa de Yesa, con atención especial a la ladera derecha. Scientific report, Ayuntamiento de Sanguesa, accesible online in. https://www.sanguesa.es/noticias/valoracion-del-dictamen-final-sobre-la-seguridad-de-las-obras-del-recrecimiento-de-la-presa-de-yesa-con-atencion-especial-a-la-ladera-derecha/.
Jaafari, A., Najafi, A., Rezaeian, J., Sattarian, A., 2015. Modeling erosion and sediment delivery from unpaved roads in the north mountainous forest of Iran. Int. J. Geomath. 6 (2), 343. https://doi.org/10.1007/s13137-014-0062-4.
Jaboyedoff, M., Carrea, D., Derron, M., Oppikofer, T., Penna, I., Bejamin, R., 2020. A review of methods used to estimate initial landslide failure surface depths and volumes. Eng. Geol. 267, 105478. https://doi.org/10.1016/j.enggeo.2020.105478.
Jaedicke, C., Van Den Eeckhaut, M., Nadim, F., et al., 2014. Identification of landslide hazard and risk 'hotspots' in Europe. Bull. Eng. Geol. Environ. 73, 325–339. https://doi.org/10.1007/s10064-013-0541-0.
Jarman, D., Harrison, S., 2019. Rock slope failure in the British mountains. Geomorphology 340, 202–233. https://doi.org/10.1016/j.geomorph.2019.03.002.
Jarman, D., Calvet, M., Corominas, J., Delmas, M., Gunnell, Y., 2014. Large-scale rock slope failures in the eastern pyrenees: identifying a sparse but significant population in paraglacial and parafluvial contexts. Geogr. Ann. Ser. B 96 (3), 357–391. https://doi.org/10.1111/geoa.12060.
Jian, X., Jianjun, W., Junjie, L., Bing, L., Xianqiun, L., Lixi, L., 2022. Mechanical properties of different lithological rocks: a case study of the coal measure strata in the eastern margin of Ordos Basin, China. Geofluids. https://doi.org/10.1155/2022/1356735.
Ju, L., Zhang, L., Xiao, T., 2023. Power laws for accurate determination of landslide volume based on high-resolution LiDAR data. Eng. Geol. 312, 106935. https://doi.org/10.1016/j.enggeo.2022.106935.
Khazaradze, G., Guinau, M., Blanch, X., Abellán, A., Tapia, M., Furdada, G., Suriñach, E., 2020. Multidisciplinary studies of the Puigcercós historical landslide in the Catalan Pyrenees. EGU General Assembly 2020. https://doi.org/10.5194/egusphere-egu2020-7796. EGU2020-7796.
Klimowitz, J., Torrescusa, S., 1990. Notas sobre la estratigrafía y facies de la serie triásica en el Alóctono Surpirenaico. In: Ortí, F., Salvany, J.M. (Eds.), Formaciones evaporíticas de la Cuenca del Ebro y cadenas periféricas, y de la zona de Levante. GPPG-ENRESA, pp. 29–33.
Lebourg, T., Zerathe, S., Fabre, R., Giuliano, J., Vidal, M., 2014. A Late Holocene deep-seated landslide in the northern French Pyrenees. Geomorphology 208, 1–10. https://doi.org/10.1016/j.geomorph.2013.11.008.
Lee, S., Min, K., 2001. Statistical analyses of landslide susceptibility at Yongin, Korea. Environ. Geol. 40 (9), 10951113. https://doi.org/10.1007/s002540100310.
Lewis, C.J., McDonald, E.V., Sancho, C., Peña, J.L., Rhodes, E.J., 2009. Climatic implications of correlated Upper Pleistocene glacial and fluvial deposits on the Cinca and Gállego rivers (NE Spain) based on OSL dating and soil stratigraphy. Glob. Planet. Chang. 67, 141–152. https://doi.org/10.1016/j.gloplacha.2009.01.001.
Liao, M., Wen, H., Yang, L., 2022. Identifying the essential conditioning factors of landslide susceptibility models under different grid resolutions using hybrid machine learning: a case of Wushan and Wuxi counties, China. Catena 217, 106428. https://doi.org/10.1016/j.catena.2022.106428.
Liu, S., Liao, C., Chen, J., Ye, G., Xia, X., 2024. Shear rate effect on clay-structure interface strength properties in various interface boundary conditions. Soil Dyn. Earthq. Eng. 177, 108389. https://doi.org/10.1016/j.soildyn.2023.108389.
López-Moreno, J.I., Soubeyroux, J.M., Gascoin, S., Alonso-Gonzalez, E., Durán-Gómez, N., Lafaysse, M., Morin, S., 2020. Long-term trends (1958–2017) in snow cover duration and depth in the Pyrenees. Int. J. Climatol. 40 (14), 6122–6136. https://doi.org/10.1002/joc.6571.
Lucia, P., 2015. Estudio de deslizamientos activos en el Valle de Tena (Huesca) mediante cartografía geomorfológica. Bachelor's Thesis.. University of Zaragoza https://zaguan.unizar.es/record/32259/files/TAZ-TFG-2015-3171.pdf.
Matte, P., 1991. Accretionary history and crustal evolution of the Variscan belt in Western Europe. Tectonophysics 196 (3–4), 309–337. https://doi.org/10.1016/0040-1951(91)90328-P.
McColl, S.T., 2012. Paraglacial rock-slope stability. Geomorphology 153-154, 1–16. https://doi.org/10.1016/j.geomorph.2012.02.015.
Migoń, P., Gutiérrez, F., Parenti, C., et al., 2023. Ebro valley gypsum escarpment near Zaragoza (NE Spain)—combination of highly valuable rock record, dynamic geomorphosites and associated cultural heritage. Geoheritage 15, 110. https://doi.org/10.1007/s12371-023-00878-x.
Montes, M.J., 2012. Mapa Geológico de España 1:50.000, Yebra de Basa. IGME, Madrid, 42 pp.
Moya, J., Romero, F., Lechón, A., Martínez, J., 2022. Modelo geológico-geotécnico actualizado de la ladera del estribo derecho de la presa de Yesa (Navarra). In: Simposio Nacional sobre Taludes y Laderas Inestables. "Taludes 2022: X Simposio Nacional sobre Taludes y Laderas Inestables", pp. 606–616. Accessible online. https://upcommons.upc.edu/handle/2117/373879.
Muñoz, J.A., 1992. Evolution of a continental collision belt: ECORS-Pyrenees crustal balanced cross-section. In: McClay, K.R. (Ed.), Thrust Tectonics. Chapman and Hall, London, pp. 247–254.
Ogita, S., Sagara, W., Higaki, D., 2017. Shapes and mechanisms of large-scale landslides in Japan: forecasting analysis from an inventory (WCoE 2014–2017). In: Sassa, K., et al. (Eds.), Advancing Culture of Living with Landslides. https://doi.org/10.1007/978-3-319-59469-9_26.
Ohazuruike, L., Lee, K.J., 2023. A comprehensive review on clay swelling and illitization of smectite in natural subsurface formations and engineered barrier systems. Nucl. Eng. Technol. 55. https://doi.org/10.1016/j.net.2023.01.007.
Pham, B.T., Bui, D.T., Prakash, I., Dholakia, M.B., 2017. Hybrid integration of multilayer perceptron neural networks and machine learning ensembles for landslide susceptibility assessment at Himalayan area (India) using GIS. Catena 149, 52–63. https://doi.org/10.1016/j.catena.2016.09.007.
Pinyol, N., Di Carluccio, G., Alonso, E., 2022. A slow and complex landslide under static and seismic action. Eng. Geol. 297, 106478. https://doi.org/10.1016/j.enggeo.2021.106478.
Pollock, W., Wartman, J., 2020. Human vulnerability to landslides. GeoHealth 4, e2020GH000287. https://doi.org/10.1029/2020GH000287.
Pérez Bielsa, C., Lambán, J., Plata, J.L., Rubio, F.M., Soto, R., 2012. Characterization of a karstic aquifer using magnetic resonance sounding (MRS) and electrical resistivity tomography (ERT): a case-study of Estaña Lakes (northern Spain). Hydrogeol. J. 20, 1045–1059. https://doi.org/10.1007/s10040-012-0839-1.
Reichenbach, P., Rossi, M., Malamud, B.D., Mihir, M., Guzzetti, F., 2018. A review of statistically-based landslide susceptibility models. Earth Sci. Rev. 180, 60–91. https://doi.org/10.1016/j.earscirev.2018.03.001.
Rodríguez Gómez, J.M., 2015. La sal y las salinas de Naval. El oro blanco del Somontano. Instituto de Estudios Altoaragoneses, Huesca, 268 pp.
Rodríguez-Méndez, L., Cuevas, J., Tubía, J.M., 2016. Post-Variscan basin evolution in the central Pyrenees: insights from the Stephanian–Permian Anayet Basin. Compt. Rendus Geosci. 348 (3–4), 333–341. https://doi.org/10.1016/j.crte.2015.11.006.
Ríos, L.M., Balera, J., Barettino, D., 1989. Memoria de la Hoja N° 145 del Mapa Geológico de España: Sallent, E. 1/50,000. ITGE, Madrid.
Rouaiguia, A., 2010. Residual shear strength of clay-structure interfaces. Int. J. Civ. Environ. Eng. 10, 5–14.
Salvany, J.M., Bastida, J., 2004. Análisis litoestratigráfico del Keuper surpirenaico central. Rev. Soc. Geol. España 17, 3–26.
Samodra, G., Ngadisih, N., Malawani, M., Mardiatno, D., Cahyadi, A., Ferman Setia, N., 2020. Frequency–magnitude of landslides affected by the 27–29 November 2017 Tropical Cyclone Cempaka in Pacitan, East Java. J. Mt. Sci. 17, 773–786. https://doi.org/10.1007/s11629-019-5734-y.
Santana Torre, V.J., 2002. El plutón de Panticosa (pirineos occidentales, Huesca): fábrica magnética y modelo de emplazamiento. Rev. Soc. Geol. Esp. 15 (3–4), 175–191.
Schönfeldt, E., Pánek, T., Winocur, D., Šilhán, K., Korup, O., 2020. Postglacial Patagonian mass movement: from rotational slides and spreads to earthflows. Geomorphology 367, 107316. https://doi.org/10.1016/j.geomorph.2020.107316.
Schuster, R.L., Highland, L.M., 2001. Socioeconomic Impacts of Landslides in the Western Hemisphere, no. August. US Department of the Interior, US Geological Survey, Denver (CO).
Selby, M.J., 1993. Hillslope Materials and Processes, 2nd edition. Oxford University Press, Oxford, p. 450.
Shi, X., Wang, L., Guo, J., Su, Q., Zhuo, X., 2019. Effects of inhibitor KCl on shale expansibility and mechanical properties. Petroleum 5, 407–412. https://doi.org/10.1016/j.petlm.2018.12.005.
Sim, K.B., Lee, M.L., Wong, S.Y., 2022. A review of landslide acceptable risk and tolerable risk. Geoenviron. Disasters 9, 3. https://doi.org/10.1186/s40677-022-00205-6.
Soldati, M., Corsini, A., Pasuto, A., 2004. Landslides and climate change in the Italian dolomites since the late glacial. Catena 55, 141–161.
Stark, T.D., Eid, H.T., 1994. Drained residual strength of cohesive soils. J. Geotech. Eng. 5, 856–871. https://doi.org/10.1061/(ASCE)0733-9410(1994)120:5(856).
Taillefer, F., 1969. Les glaciations des Pyrénées. Bull. AFEQ., INQUA, Paris, pp. 19–32.
Tebbens, S.F., 2020. Landslide scaling: a review. Earth Space Sci. 7, e2019EA000662. https://doi.org/10.1029/2019EA000662.
Valenzuela, P., Domínguez-Cuesta, M.J., García, M., Jiménez-Sanchez, M., 2017. A spatio-temporal landslide inventory for the NW of Spain: BAPA database. Geomorphology 293. https://doi.org/10.1016/j.geomorph.2017.05.010.

Van Westen, C.J., Van Asch, T.W.J., Soeters, R., 2006. Landslide hazard and risk zonation—why is it still so difficult? Bull. Eng. Geol. Environ. 65 (2), 167–185. https://doi.org/10.1007/s10064-005-0023-0.

Varnes, D.J., 1978. Slope movement types and processes. In: Schuster, R.L., Krizek, R.J. (Eds.), Landslides, Analysis and Control, Special Report 176: Transportation Research Board. National Academy of Sciences, Washington, DC, pp. 11–33.

Waltham, T., Bell, F., Culshaw, M., 2005. Sinkholes and Subsidence. Karst and Cavernous Rocks in Engineering and Construction. Springer, Chichester, United Kingdom, 373 pp.

Wilde, M., Günther, A., Reichenbach, P., Malet, J.P., Hervás, J., 2018. Pan-European landslide susceptibility mapping: ELSUS Version 2. J. Maps 14 (2), 97–104. https://doi.org/10.1080/17445647.2018.1432511.

Xu, Q., Li, Y., Zhang, S., Dong, X., 2016. Classification of large-scale landslides induced by the 2008 Wenchuan earthquake, China. Environ. Earth Sci. 75, 22. https://doi.org/10.1007/s12665-015-4773-0.

Yang, X., Li, J., Zhang, Y., Lei, J., Li, X., Huang, X., Xu, C., 2024a. Experimental study on mechanical properties of anisotropic slate under different water contents. Appl. Sci. 14, 1473. https://doi.org/10.3390/app14041473.

Yang, Y., Peng, S., Huang, B., Xu, D., Yin, Y., Li, T., Zhang, R., 2024b. Multi-scale analysis of the susceptibility of different landslide types and identification of the main controlling factors. Ecol. Indic. 168, 112797. https://doi.org/10.1016/j.ecolind.2024.112797.

Yi, Y., Xiwei, X., Guangyu, X., Huiran, G., 2023. Landslide detection using time-series InSAR method along the Kangding-Batang section of Shanghai-Nyalam road. Remote Sens. 15, 1452. https://doi.org/10.3390/rs15051452.

Zarroca, M., Linares, R., Roqué, C., Rosell, J., 2013. Integrated geophysical and morphostratigraphic approach to investigate a coseismic (?) translational slide responsible for the destruction of the Montclus village (Spanish Pyrenees). Landslides 11, 655–671.

Zhao, B., Wang, Y., Luo, Y., Liang, R., Li, J., Xie, L., 2019. Large landslides at the northeastern margin of the Bayan Har Block, Tibetan Plateau, China. R. Soc. Open Sci. 6, 180844. https://doi.org/10.1098/rsos.180844.

Zhou, S., Chen, Chen, G., Ligang, F., 2016. Distribution pattern of landslides triggered by the 2014 Ludian earthquake of China: implications for regional threshold topography and the seismogenic fault identification. Int. J. Geo-Inf. 5, 46. https://doi.org/10.3390/ijgi5040046.